SEMIANNUAL STATUS REPORT

for

Computer Simulation of Surface and Film Processes

May 1, 1983 - October 31, 1983

Cooperative Agreement No.: NCC 2-125

Period of Award: May 1, 1981 - April 30, 1984

Principal Investigator: Professor W. A. Tiller

Senior Investigator: Dr. M. T. Halicioglu

SU-DMS-84-R-2

Stanford/NASA Ames Joint Institute for Surface and Microstructure Research
Department of Materials Science and Engineering
Stanford University, Stanford, CA 94305

COMPUTER SIMULATION OF SURFACE AND FILM PROCESSES

In this report the results obtained in two separate investigations are presented:

(i) Simulation studies based on a potential comprising two-body and three-body interactions. As model systems, several different silica phases are taken into consideration.

(ii) Crack propagation studies in two-dimensional triangular lattices.

The progress made in these areas during this period is given in the following two self-contained chapters.

CHAPTER I.

Simulation studies based on a potential with two- and three-body interactions. Crystalline silica phases, their surfaces and interfaces were modeled.

INTRODUCTION

Using computer simulation techniques, the behavior of a model system (with many degrees of freedom) can be computed to analyze various physical phenomena. It has been shown that adequate computer methods, based on interactions between discrete particles, can provide information leading to an atomic level understanding of various processes [1-7]. The success of these simulation methods, however, is closely related to the accuracy of the potential energy function representing the interactions among the particles. The prime objective of the present investigation is to develop a potential energy function for crystalline SiO_2 forms that can be employed in lengthy computer modelling procedures. Such a potential energy function which could furnish acceptable crystalline forms of SiO_2 at finite temperatures (say, under a Monte Carlo or molecular dynamics code) presently is unavailable. In many of the simulation methods which deal with discrete particles, semi-empirical two-body potentials have been employed to analyze energy and structure-related properties of the system [1-10]. However, it is now well accepted that many-body interactions are required for a proper representation of the total energy for many systems. There are numerous reports indicating the significance of multi-body interactions in calculating energy and structure-related properties[11-19]. In this study, we included many-body interactions in an appropriate way for simulations based on discrete particles.

In general, for a system of N particles, the total potential energy may be expanded as [15]:

$$\Phi = \frac{1}{2!}\sum_{i}^{N}\sum_{\substack{j\\ i\neq j}}^{N} u(\vec{r}_i,\vec{r}_j) + \frac{1}{3!}\sum_{i}^{N}\sum_{\substack{j\\ i\neq j\neq k}}^{N}\sum_{k}^{N} u(\vec{r}_i,\vec{r}_j,\vec{r}_k) + \cdots$$

$$\cdots + \frac{1}{n!}\sum_{i}^{N}\sum_{j}^{N}\cdots\sum_{\substack{n\\ i\neq j\neq\cdots\neq n}}^{N} u(\vec{r}_i,\vec{r}_j,\cdots,\vec{r}_n) + \cdots \qquad (1)$$

where, $u(\vec{r}_i,\vec{r}_j)$, $u(\vec{r}_i,\vec{r}_j,\vec{r}_k)$, ..., $u(\vec{r}_i,\vec{r}_j,..,\vec{r}_n)$ are two, three, and n-body potentials, respectively. The position of the i'th particle is denoted by $\vec{r}_i$.

Clearly, the most important term in this expansion is the first term involving two-body interactions. Therefore, in the majority of the atomistic calculations made to date, only pairwise additive potentials have been used. This provides great simplification in the analytical formalism as well as in numerical computations. When the parameters of a two-body potential, however, are calculated from, say, an experimentally determined

bulk property, the pairwise nonadditive (i.e, multi-body) contribution to the total energy is introduced indirectly via estimated parameters in a complicated way. The two-body potential, therefore, with parameters carrying the effect of the many-body portion of the total potential is called an "effective" pair potential [14,15,20]. In general, effective potentials provide good results when another property of the same state is calculated (i.e., as long as variations in the local atomic configuration remain negligible) [21]. However, if the properties of another state have to be calculated, the many-body part should be included in a theoretically acceptable way, if its contribution is considerable [20].

In this investigation, energy and structure-related properties for systems containing Si and O atoms were taken into consideration. Simulations were performed at finite temperatures using a Monte Carlo procedure. For total energy calculations, both two-body and three-body interactions were taken into account. Reported model calculations for energy and structure-related properties of systems with Si and O atoms are rather scarce [22-26]. In general, all these earlier calculations were carried out assuming only two-body "effective" potentials. An ionic model based on the Born-Meyer-Huggins potential (which is an "effective" pair potential in nature) was adopted for this purpose [27]. For several macroscopic properties, in particular for the representation of amorphous structures, this potential function produced very interesting results which are consistent with experiments. However, at the present time, there is no indication that this potential would allow various crystalline SiO_2 structures to be stable [1].

In the present study, with a potential energy function comprising two and three-body interactions, we were able to obtain stable crystalline structures for low and high temperature forms of quartz and cristobalite employing a Monte Carlo procedure. The results emphazise the importance of multi-body interactions in the stability of crystalline SiO_2 phases.

POTENTIAL ENERGY FUNCTION

To calculate the total potential energy of a system in a given configuration, equation 1 was employed considering two-body and three-body interactions. Four and higher body terms, however, were neglected. Because this expression (equation 1) had to be used in lengthy machine computations, $u(\vec{r}_i, \vec{r}_j)$ and $u(\vec{r}_i, \vec{r}_j, \vec{r}_k)$ were chosen with the simplest possible functional forms. In this study, therefore, the two-body part was represented by a Mie-type potential which is given by:

$$u(r_{ij}) = \frac{\epsilon}{(m-n)} \left(n(\frac{r_o}{r_{ij}})^m - m(\frac{r_o}{r_{ij}})^n \right) \qquad (2)$$

with, $r_{ij} = |\vec{r}_i - \vec{r}_j|$, r_o denotes the equilibrium separation and ϵ is the energy at $r_{ij} = r_o$. The exponents m and n account for the repulsive and attractive terms, respectively. The three-body part, on the other hand, was expressed as:

$$u(\vec{r}_i, \vec{r}_j, \vec{r}_k) = \sum_l Z_l \cdot G_l(\vec{r}_i, \vec{r}_j, \vec{r}_k) \tag{3}$$

where, the summation includes all triple multipole interactions resulting from the expansion of the third-order interaction energy for three atoms. Each term in the summation is expressed as the product of a geometrical factor $G(\vec{r}_i, \vec{r}_j, \vec{r}_k)$ which depends on the relative positions of the three atomic nuclei and an interaction constant which depends only on the atomic species involved in the interaction. The functional forms of $G(\vec{r}_i, \vec{r}_j, \vec{r}_k)$ for several multiple interactions have been obtained by Bell [28]; and by Doren and Zucker [29]. Here, we consider only the triple-dipole interaction which has been shown to be the dominant contribution [30,31]. This term was first obtained for closed shell atoms by Axilrod and Teller [31] as:

$$u(\vec{r}_i, \vec{r}_j, \vec{r}_k) = Z_1 \cdot G_1(\vec{r}_i, \vec{r}_j, \vec{r}_k) \tag{4}$$

with

$$G_1(\vec{r}_i, \vec{r}_j, \vec{r}_k) = \frac{1 + 3Cos\theta_i Cos\theta_j Cos\theta_k}{(r_{ij} \cdot r_{ik} \cdot r_{jk})^3} \tag{5}$$

where, $\theta_i, \theta_j, \theta_k$ and r_{ij}, r_{ik}, r_{jk} represent the angles and the sides of the triangle formed by the three particles i, j and k. Parameters such as ϵ, r_o, m, n and Z will be referred to as "internal" parameters indicating that they depend only on the atomic characteristics of the corresponding particles.

Now, combining equations 1 through 5, and neglecting the four-body and higher terms, one obtains:

$$\Phi = \Psi_2 + \Psi_3 \tag{6}$$

with

$$\Psi_2 = \frac{1}{2} \sum_i^N \sum_{\substack{j \\ i \neq j}}^N \frac{\epsilon}{(m-n)} \left(n(\frac{r_o}{r_{ij}})^m - m(\frac{r_o}{r_{ij}})^n \right) \tag{7}$$

and

$$\Psi_3 = \frac{1}{6}\sum_{i}^{N}\sum_{\substack{j \\ i\neq j\neq k}}^{N}\sum_{k}^{N} Z_1 \cdot \left(\frac{1 + 3Cos\theta_i Cos\theta_j Cos\theta_k}{(r_{ij} \cdot r_{ik} \cdot r_{jk})^3}\right) \tag{8}$$

In this general form, the total potential energy Φ is a function of the atomic coordinates, and the internal parameters. These parameters, as mentioned above, are assumed to be independent of the atomic positions and the geometry of the system; they depend only on the atomic properties of the species involved.

For a binary system of types 1 and 2 with the corresponding number of particles N_1 and N_2 (for example, for the SiO_2 case), equations 7 and 8 may be rewritten as:

$$\Psi_2 = \sum_{\alpha}^{2}\sum_{\beta}^{2} \frac{N_\alpha \cdot \epsilon_{\alpha\beta}}{2(m_{\alpha\beta} - n_{\alpha\beta})}\left[n_{\alpha\beta} \cdot a_{\alpha\beta}^{(m_{\alpha\beta})} \cdot R_{\alpha\beta}^{(m_{\alpha\beta})} - m_{\alpha\beta} \cdot a_{\alpha\beta}^{(n_{\alpha\beta})} \cdot R_{\alpha\beta}^{(n_{\alpha\beta})}\right] \tag{9}$$

with $\alpha = 1, 2$, $\beta = 1, 2$ and $\gamma = 1, 2$; and

$$\Psi_3 = \sum_{\alpha}^{2}\sum_{\substack{\beta \\ \beta<\gamma}}^{2}\sum_{\gamma}^{2} \frac{N_\alpha Z_{\alpha\beta\gamma}}{3d^9} \cdot T_{\alpha\beta\gamma} \tag{10}$$

where,

$$R_{\alpha\beta} = \frac{r_{o\alpha\beta}}{d} \tag{11}$$

$$a_{\alpha\beta}^{(m_{\alpha\beta})} = \sum_{j}^{N_\beta}\left(\frac{d}{r_{\alpha j}}\right)^{m_{\alpha\beta}} \tag{12}$$

$$a_{\alpha\beta}^{(n_{\alpha\beta})} = \sum_{j}^{N_\beta}\left(\frac{d}{r_{\alpha j}}\right)^{n_{\alpha\beta}} \tag{13}$$

and

$$T_{\alpha\beta\gamma} = \sum_{j}^{N_\beta}\sum_{\substack{k \\ j<k}}^{N_\gamma} G(r_{\alpha i}, r_{\alpha j}, r_{\alpha k}) \tag{14}$$

with, $r_{\alpha i} \neq 0$, $r_{\alpha j} \neq 0$ and $r_{\alpha k} \neq 0$; (and considering $r_{\alpha\beta} = r_{\beta\alpha}$). Here, $r_{o\alpha\beta}$ represents the equilibrium separation between the two species α and

β for the two-body part ; d is a critical distance parameter which is used as a normalizing factor. Φ is independent of the value of d. $r_{\alpha j} = |\vec{r}_\alpha - \vec{r}_j|$, where, $\vec{r}_\alpha$ denotes the position of an atom of type α taken as the central particle for the summation. The total number of particles in the system is given by $N_{Tot} = N_1 + N_2$; while, $m_{\alpha\beta}$ and $n_{\alpha\beta}$ are the exponents for the repulsive and attractive parts of the two-body potential.

The Mie potential (equation 2) which is employed to represent "bare" two-body interactions is the general form of the commonly used Lennard-Jones potential with m and n assumed to be equal to 12 and 6, respectively. Here, m and n determine the curvature of the function around the minimum and would provide a greater flexibility, in particular, when left as variables in calculating quantities expressed as derivatives of the potential energy. Even though the Mie potential may represent "bare" two-body potentials fairly well, an accurate representation of the three-body part is more difficult to attain. Only a limited number of reports can be found in the literature proposing an analytic formula for three-body interaction which would meet our requirements. In this first attempt, we adopted the Axilrod-Teller approach to analyze, at least, some of the generic features produced by a formal three-body function in the calculation of structural and energy-related properties for various SiO_2 crystals.

The functional representation of Φ as sums of two and three-body terms is quite different from the usual formulation of the total potential energy as a sum of "effective" two-body potentials alone. In the present formalism $u(\vec{r}_i, \vec{r}_j)$ is the "bare" two-body potential and the many-body effect is introduced via $u(\vec{r}_i, \vec{r}_j, \vec{r}_k)$. In the "effective" pair potential formalism, however, the many-body part is incorporated with the two-body 'internal' parameters, therefore, the muiti-body part was implicitly assumed to be pairwise additive. This assumption, in turn, makes the 'internal' potential parameters very much more locally structure dependent (i.e.,for another geometrical arrangement of atoms, for instance, going from bulk to the surface, adjustments in the parameters would be necessary). At this point, it is anticipated that the present formalism of the total energy as sums of "bare" two-body plus three-body interactions would cause the internal parameters to become much less position and geometry dependent than in the case of an "effective" two-body approximation. See appendix 1.

CALCULATION OF THE PARAMETERS

For a binary system such as SiO_2, evaluation of the parameters (internal parameters, in particular) constituted the most cumbersome part of this investigation. We used only experimental data to evaluate these parameters. The total potential energy of a binary system as given by equations 6 and 9

through 14 contains two classes of parameters. (i) Internal parameters which are related implicitly to the atomic properties (such as the polarizability, mean excitation energy and atomic volume) of the species involved in the interaction. (ii) Geometric (external) parameters, as given by equations 12 through, 14 are functions of atomic positions and depend solely on the configuration of the system. These geometric parameters are basically some kind of lattice sums and, for known crystalline structures, can easily be calculated. Table 1 tabulates these parameters for several crystalline SiO_2 forms. Internal parameters, on the other hand, are more difficult to evaluate. In contrast to the geometrical parameters which are dependent on the configuration, internal parameters are assumed to be independent of the habit and the geometrical setting of the system. Therefore, the same set of internal parameters which reproduces experimental quantities satisfactorly, say for the pure Si, can be employed for calculating the two and three-body interactions among Si atoms in any SiO_2 form. The total potential energy, Φ, expressed by equation 6 is, by definition, the cohesive energy of the system. This constitutes one of the main expressions in the internal parameters evaluation procedure. The other major relation that has been used is the stability relation given by:

$$\frac{\partial \Phi}{\partial V} = 0 \qquad (15)$$

where, V denotes the total volume of the system. Obviously, this expression is exact only at static equilibrium (i.e., at T =0°K). However, it has been, generally, assumed that the minimum of $\Phi(V)$ coincides with the minimum of the free energy of the system as a function of V.

For a binary system such as SiO_2, the internal parameters can be partitioned into three groups. (i) Parameters for pure silicon: Experimental small cluster and bulk data for Si were used to calculate pure silicon parameters [32,33]. Equation 6 has been employed in this evaluation assuming $m_{(Si-Si)} = 12$ and $n_{(Si-Si)} = 6$. The two body energy well depth for equation 2 was calculated as $\epsilon_{(Si-Si)} = 37740.0°K$ based on the reported experimental dissociation energy of the Si_2 molecule. The standard enthalpy of vaporization for the crystalline Si has been reported as 56900 ± 1500°K [33]. This value was used in equation 1 as an input (a small term of the order of PV has been neglected, here, and cohesive energy $\approx -H_{(vap)}$ has been assumed). Then, the solution of equation 1 based on the stability criterion (equation 15) produced: $r_{o(Si-Si)} = 2.2134\ \mathring{A}$ and $Z_{(Si-Si-Si)} = 5.2934 \times 10^7 (°K\mathring{A}^9)$. This set of parameters reproduces the correct energy and structure for the crystalline silicon, as well as the reported microcluster data (i.e., energy and the structure) for Si_2 and Si_3. Furthermore, the diamond structure for the bulk Si satisfies the stability

criterion and was found to have a lower energy than either the hcp, fcc or bcc structures. These parameters, however, were not tested for reproducing quantities expressed as higher derivatives of Φ. (ii)Parameters for pure oxygen: Considering the dissociation energy of the O_2 molecule, the two-body potential well depth for equation 2 was taken as $\epsilon_{(O-O)} = 59943.0$ (^oK) [34]. The exponents in the two-body function were assumed to be $m_{(O-O)} = 12$ and $n_{(O-O)} = 6$. Based on spectroscopic data the equilibrium distance between two O atoms was taken as the average bond length for the O_2 molecule, $r_{o(O-O)} = 1.208$ $\mathring{A}$ [34]. In this case no bulk data (for example, based on solid oxygen) was employed to calculate the three-body intensity parameter. Instead, we used reported ozone (O_3) data [35] and obtained $Z_{(O-O-O)} = 2.622 \times 10^5$ ($^oK\mathring{A}^9$). These parameters for pure oxygen are, now, exact for the minimum point of the two-body potential curve and provide good dissociation energy for O_3. However, minimization of the total energy yields a linear O_3 molecule. At this point no further attempt has been made to correct this shortcoming by refining the parameters. (iii) Cross parameters: in the calculation of the cross parameters (i.e., for interaction between Si and O atoms) experimental data from bulk α-cristobalite and α-quartz were employed. In this case, again by assuming $m_{(Si-O)} = 12$ and $n_{(Si-O)} = 6$, we are left with four cross parameters ($\epsilon_{(Si-O)}, r_{o(Si-O)}, Z_{(Si-Si-O)}$ and $Z_{(Si-O-O)}$) to be determined. The cohesive energies for α-cristobalite and α-quartz were obtained from standard enthalpies of formation which are tabulated in Table 2. These experimental cohesive energies for α-cristobalite and α —quartz were employed in equation 6 in determining the parameters. Now, equation 6 and 15 for α-cristobalite and α-quartz constitute four "nonlinear" simultaneous equations. However, in these simultaneous equations, the coefficients for the corresponding terms are numerically very similar, and this makes acceptable roots difficult to obtain. To overcome this undesired "ill condition" situation and, at the same time, to investigate the effect of the input values of cohesive energies on the parameters, the values of Φ's for both α-cristobalite and α-quartz were varied within limits of the experimental error margin. It was found that, in general, small variations in Φ produces acceptable roots. So far, we have considered only positive roots. Table 3 tabulates calculated values for the cross parameters using two different sets of cohesive energies (varied within experimental limits), along with the parameters for pure systems.

COMPUTATIONAL PROCEDURE AND RESULTS

Employing parameters obtained in the preceding section, simulation calculations were carried out at finite temperatures for α-cristobalite, α-quartz, β-cristobalite and β-quartz. (These four allotropic crystalline forms of SiO_2 will be referred as $\alpha - c$, $\alpha - q$, $\beta - c$ and $\beta - q$, respectively). In this investigation we are mostly concerned about the structural stability of these four SiO_2 forms under a Monte Carlo code based on a potential function given by equation 6. The stability criterion imposed by equation 15 in calculating internal parameters may only be valid at the static limit (i.e., at $T = 0^{\circ}K$). This condition, therefore, can not necessarly guaranty the preservation of the proper symmetry and configuration of the system at a finite temperature.

Model calculations were performed using a Monte Carlo technique based on the Metropolis approximation [36-38]. This is a stochastic method weighted according to the Boltzmann factor. In this procedure, every particle is treated discretely at finite temperatures. In general, the particles were positioned initially according to the crystalline structure of the system under consideration. Then, every atom was displaced by a self-adjusting step size. The acceptance of the new position is decided by the Metropolis procedure which is employed for every particle in the system based on the temperature and the particle's total energy. This technique generates a series of snapshots representative of the energetically most probable region of the phase space and, in principle, it can provide ensemble averages of any position-dependent quantity.

Throughout this investigation, calculations were performed considering the same internal parameters for pure silicon and pure oxygen. In the case of the cross parameters we used set #1, as given in Table 2; occasionally, however, set #2 was employed for parallel runs to investigate the effect caused by the cross parameters on the final result. This analysis, namely, the investigation of the effect of the parameters on the calculated macroscopic characteristics of the system, at the moment, is incomplete. However, the present study indicates that they are extremely important in understanding the intricate relationship between atomic properties and the structural characteristics of the system.

First, the bulk structures of the four different SiO_2 forms ($\alpha - c$, $\alpha - q$, $\beta - c$ and $\beta - q$) were simulated. The temperature was taken as 300 'K and the initial configuration for each system was generated based on its reported crystallographic data [39-41]. For calculating bulk properties, a three-dimensional periodic boundary condition was imposed on the systems to eliminate the surface effect [42]. The volume of the computational box was taken somewhat larger than $1000\mathring{A}^3$ depending on the crystalline structure

of the system. The potential energy cut-off radius, R_{cut}, was taken typically as 5.0$\mathring{A}$. In order to analyze the effect of the R_{cut} on the final result, the calculation for $\alpha - c$ was repeated with $R_{cut} = 7.0\mathring{A}$, but no appreciable difference in either the total energy or in the final atomic configuration was detected. All iterations were carried out until complete equilibration, which was monitored by the variation in the total potential energy. In general, equilibrations were attained before 5000 iteration steps. For all the four SiO_2 forms studied, it has been found that equilibrated structures preserved their original symmetry very well. The orientation of atoms in these equilibrated structures was analyzed by the radial distribution function (RDF), and by the angular distribution function (ADF).

The RDF provides mean peak positions for $d_{(Si-O)}$, $d_{(O-O)}$ and $d_{(Si-Si)}$ corresponding to first neighbor distances between $Si-O$, $O-O$ and $Si-Si$ atoms. As an example, figure 1 demonstrates the calculated total RDF for the $\alpha - c$ case. At 300°K, the mean peak positions for all four cases remained virtually unaffected (with respect to the initial first neighbor distances based on the crystallographic data). Due to thermal fluctuations, however, the peaks became more diffuse, as anticipated. The most pronounced relaxation took place for the $Si-O$ peak of $\beta - c$ for which we considered the ideal structure as the initial configuration. The equilibration, in this case, caused a shift for $d_{(Si-O)}$ from 1.71 to 1.57 (to 1.58 for the cross parameter set #2), which is in the right direction toward the experimental value of 1.612 for the real $\beta - c$ [39]. Furthermore, the RDF mean peak positions were found to be quite insensitive to the type of cross parameters employed in the relaxation procedure (see Table 4).

The ADF was used to analyze average $Si-O-Si$ and $O-Si-O$ angles formed by the nearest neighbors of the corresponding atoms. These angles are found to be very useful in the characterization of various SiO_2 forms [25,39]. In all four cases investigated here, averaged values of the $O-Si-O$ angle, which is the internal angle of the SiO_4 tetrahedron, was found to be around 109 degrees. This is consistent with many experimental findings. The intra-tetrahedral angle, $Si-O-Si$, however exhibits some variations among the allotropic forms of SiO_2 considered. As an example, Figure 2 demonstrates the ADF for $Si-O-Si$ and $O-Si-O$ of $\alpha - c$. The effect of the type of cross parameters was found to be somewhat more visible on the average value of the $Si-O-Si$ angle when compared with the effect on the averaged $O-Si-O$ angle. In general, cross parameter set #1 provides slightly larger $Si-O-Si$ angles (see Table 4 for comparison).

Calculated cohesive energies for the equilibrated SiO_2 forms are given in Table 2, along with the experimental values. All the calculated cohesive energies were found to be within acceptable limits. The effect of different

cross parameters on the calculated total energies is noticeable but quite small and the calculated energies remained within experimental error margins.

Next, we performed simulation calculations for (001) surfaces of the $\alpha - c$. Again, the Monte Carlo method based on equation 6 was employed considering the same set of parameters, as above. Initially, exposed surfaces were generated by cutting an ideal $\alpha - c$ crystal in the (001) direction. This was accomplished by imposing periodic boundary conditions only in the x and y-directions for a properly positioned crystal that produced "infinite" exposed surface planes in both $+z$ and $-z$ directions. One obtains a "regular" surface structure when the cutting plane is located between two neighboring O-planes in the (001) direction. Otherwise, depending on the location of the cutting plane, the surface created would be O-rich in one side and Si-rich in the other. Equilibration runs were carried out (i)for a regular surface and (ii) for an O-rich surface, considering systems with 96 moving atoms at T= $300^{o}K$.

The reconstruction for the "regular" surface was found to be minimal. The largest displacement was exhibited by the top O atoms which expanded outwards approximately $0.7\mathring{A}$. At the same time these top layer O atoms moved slightly toward the nearest Si atoms. Top and side views for the regular surface are shown in Figure 3 before and after equilibration. Equilibrated surface configurations obtained using cross set #1 and set #2 were virtually identical. However, the effect of the cross parameters was very pronounced in the surface energy calculations. Cross parameter set #1 produced a surface energy of 841.6 mJ/m^2 which is in a good agreement with experimental findings [43]. Set #2, on the other hand, yielded a negative surface energy value (-310.0 mJ/m^2) which is in obvious disagreement.

The O-rich surface for the $\alpha - c$ exhibited considerable surface reconstruction. O atoms located in the top layer (i.e., excess O atoms) moved closer to O atoms of the neighboring tetrahedron (located slightly lower than the excess O atoms) forming so called peroxide bridges. Figure 4 shows the schematic representation of the reconstructed O-rich (001) surface of $\alpha - c$. Formation of these peroxide bridges has already been determined by several investigators [44,45].

DISCUSSION AND CONCLUSIONS

The effect introduced by three-body interactions is quite pronounced and complex. In contrast to two-body interactions, three-body forces encourage open structures. Therefore, in the present formalism the familiar picture of pairwise additive interacting particles, which favors compact

structures, is drastically altered. For example, the behavior of the O atoms in the SiO_2 crystals represent this three-body effect quite clearly. The internal parameters used for the pure oxygen two-body potential were chosen to reproduce the equilibrium O_2 data correctly. Accordingly, in the two-body potential part for pure O we have $r_{o(O-O)} = 1.208$ Å (see above). In the simulation runs for crystalline SiO_2 forms, the average nearest neighbor $O - O$ distance was found to be around 2.59 Å . Strong three-body interactions, due to surrounding Si or other O atoms in the bulk prevented the O atoms from further approaching each other (despite thermal motions introduced by the Monte Carlo code employed). At the O-rich surface, on the other hand, due to a "reduced" three-body effect, the top O atoms can come closer to form peroxide bridges.

The present interaction potential function does not utilize any covalency or ionicity concepts, nor does it catagorize the interactions between particles into short or long range. This concept, although it may be quite useful in many other modelling procedures, would be rather difficult to assess, in particular, at the surface region or in the vicinity of a defect.

One of the most important outcomes of the present investigation is the fact that three-body potentials, even in a simple analytic form (but, adequately represented by triplet summation), can provide stable SiO_2 crystalline forms involving thermal fluctuations. This work, in this respect, may be regarded as a first attempt at investigating the multi-body effect in the energetics and structure-related properties of SiO_2 phases. Calculated potential energy parameters reported in this paper represent only a sample case for comparison. The test for the ability of these parameters to reproduce other macroscopic quantities of the corresponding compounds is an enormous job that was only performed partly in this investigation. Therefore, reported numerical results may be only semi-qualitative in nature, and should be treated accordingly.

The computational time required for these simulation runs were considerably higher than the usual calculations based on two-body interactions alone. For example, an equilibration run for a system containing approximately 200 relaxing particles may take up to an hour of CPU time in a CDC 7600 machine. The largest part of this computation time is spent to calculate the three-body interactions. Despite this relatively long computer time requirement, simulation runs for SiO_2 systems based on the present potential energy function are well within reach.

APPENDIX 1.

In the present model the 'bare' two-body potential, $u(r_{ij})$ for a particular pair is always represented with the same functional form associated with the same parameters irrespective of the immediate surrounding. The effect of the neighboring particles (which is the many- body effect) is accounted for via the three-body term. Therefore, the evaluation of the two-body part can be accomplished using simply diatomic data. However, extreme care must be exercised in extracting such information from approximate ab initio calculation results.

For any given two atoms the "bare" two-body potential is a function of the internuclear separation, r_{ij}, and formally it may be defined as:

$$u(r_{ij}) = E(r_{ij}) - E(r_{ij\infty}) \qquad A1$$

where, $E(r_{ij})$ and $E(r_{ij\infty})$ denote the total ground state energies for the two particles at a separation r_{ij} and at an infinitely large internuclear separation, respectively. Based on first principle quantum mechanical considerations, $E(r_{ij})$ and $E(r_{ij\infty})$ may be exactly calculated by:

$$E(r_{ij}) = E^{(HF)}(r_{ij}) + E^{(CORR)}(r_{ij}) \qquad A2$$

$$E(r_{ij\infty}) = E^{(HF)}(1) + E^{(CORR)}(1) + E^{(HF)}(2) + E^{(CORR)}(2) \qquad A3$$

where, $E^{(HF)}(r_{ij})$ and $E^{(CORR)}(r_{ij})$ are the total Hartree-Fock and electronic correlation energies for the two particles at a separation r_{ij}, and $E^{(HF)}(1)$, $E^{(CORR)}(1)$ and $E^{(HF)}(2)$, $E^{(CORR)}(2)$ denote corresponding energies for the isolated particles 1 and 2, respectively. In the absence of any external field, both $E(r_{ij})$ and $E(r_{ij\infty})$ represent the lowest energy level for the corresponding systems. Accordingly, the function $u(r_{ij})$ can be derived continuously from the long range dispersion limit to the short range steep repulsion region which also covers the region around the minimum. Obviously, the quantum theory for such a curve does not require separate approaches for the long and short range regions.

In particular, for many electron systems, an exact evaluation of $u(r_{ij})$ based on first principles, at the moment, is not possible due to various computational difficulties. To overcome some of these inherent difficulties, various approximate methods have been proposed. In the majority of these methods for calculating $u(r_{ij})$ involving many electron systems, one generally assumes a particular hybrid type for the bonding between the atoms. Accordingly, calculations produce a $u(r_{ij}, h)$ curve which is a two-body potential curve for the particular hybrid type imposed. For different

hybrid types one obtains a series of $u(r_{ij}, h)$ curves some of which may coincide with $u(r_{ij})$ for a certain range of r_{ij}. In principle, the lower envelope the these $u(r_{ij}, h)$ curves must coincide with $u(r_{ij})$ of equation A1.

ACKNOWLEDGEMENTS

This work was supported, in part by the Defence Advanced Research Project Agency under Contract numbers MDA 903-79-C0484 and MDA 903-83-K-0041, and in part by NASA, Ames Research Center via Contract #NCC2-125.

References

1. "Computer Simulation of Solids", Eds: C. R. A. Catlow & W.C. Mackrodt, (Lecture Notes in Physics); 166, Springer-Verlag (1982).
2. J. R. Beeler, Jr. and G. L. Kulcinski, "Interatomic Potentials and Simulation of Lattice Defects", Eds: P. G. Gehlen, J. R. Beeler, Jr., and R. I. Jaffee(Plenum Press, New York, 1972).
3. "Computer Simulation for Materials Application", Eds: R. J. Arsenault, J. R. Beeler, Jr. and J. A. Simmons. Nuclear Metallurgy, Vol. 20 (National Bureau of Standards, Maryland, 1976).
4. "An Introduction to Computer Simulation in Applied Science", Eds: F. Abraham and W. A. Tiller(Plenum Press, New York, 1972).
5. R. Bennett, "Diffusion in Solids, Recent Developments", Eds: A. S. Nowick and J. J. Burton(Acad. Press, New York, 1975), Ch. II.
6. T. Halicioglu, J. Cryst. Growth 29, 40 (1975).
7. D. W. Bassett and P. R. Weber, Surf. Sci. 70, 520 (1978).
8. T. Halicioglu, J. Cryst. Growth 33, 212 (1976).
9. T. Halicioglu and H. Poppa, Proc. 7th Intern. Vac. Congr and 3rd Intern Conf. on Solid Surfaces (Vienna, 1977), p. 1113.
10. T. Halicioglu, Surf. Sci. 79, L346 (1979).
11. T. Halicioglu, Phys. Stat. Sol. (b) 99, 347 (1980).
12. T. Halicioglu and P. J. White, J. Vac. Sci. Tech. 17, 1213 (1980).
13. J. Schmit, Surf. Sci. 55, 589 (1976).
14. "Intermolecular Forces", Eds: J. O. Hirschfelder , Adv. Chem. Phys., Vol. 12 (1967).
15. O. Sinanoglu, Adv. Chem. Phys. 12, 283 (1967).
16. K. F. Niebel and J. A. Venables, "Rare Gas Solids", Eds: M. L. Klein and J. A. Venables, (Acad. Press, 1976), Ch. 9.
17. T. L. Einstein, Surf. Sci. 84, 1497 (1979).
18. C. Hoheisel, Phys. Rev. (A) 23, 1998 (1981).
19. J. W. Martin, J. Phys. C: Solid State Phys. 8, 2859 (1975); see also, 8, 2869 (1975).
20. H. Margenau and N. R. Kestner, "Theory of Intermolecular Forces" (Pergamon Press, 1971).
21. R. Duren, Adv. Atomic and Molec. Phys. 16, 55 (1980).

22. S. K. Mitra, M. Amini, D. Fincham and R. W. Hockney, Phil. Mag. (B) **43**, 365 (1981).

23. L. V. Woodcock, C. A. Angell and P. Cheeseman, J. Chem. Phys. 65, 1569 (1976).

24. T. F. Soules, J. Chem. Phys. **71**, 4570 (1979).

25. S. K. Mitra, Phil. Mag. (B) **45**, 529 (1982).

26. S. H. Garofalini, J. Chem. Phy. **78**, 2069 (1983).

27. W. R. Busing, J. Chem. Phys. **57**, 3008 (1972).

28. R. J. Bell, J. Phys. (B) **3**, 751 (1970).

29. M. B. Doran and I. J. Zucker, J. Phys. (C) **4**, 307 (1971).

30. R. J. Bell and I. J. Zucker, "Rare Gas Solids", Eds: M. L. Klein and J. A. Venables, (Acad. Press, 1976), Ch. 2.

31. B. M. Axilrod and E. Teller, J. Chem. Phys. **11**, 299 (1943).

32. G. Verhaegen, F. E. Stafford, and J. Drowart, J. Chem. Phys. 40, 1622 (1964).

33. J. Drowart, G. De Maria and M. G. Inghram, J. Chem. Phys. **29**, 1015(1958).

34. D. R. Stull, et al. "Thermodynamic Prop. of Elements", Advances in Chem. Ser., NO.18, Washington (1956).

35. "Physical Constants of Ozone & Oxygen", Armour Res. Foundation, (1958).

36. F. James, Rep. Prog. Phys. **43**, 1146 (1980).

37. W. W. Wood and J. J. Erpenbeck, Ann. Rev. Phys. Chem. **27**, 319 (1976).

38. N. Metropolis, A. W. Rosenbluth, M. N. Rosenbluth, A. H. Teller and E. Teller, J. Chem. Phys. **21**, 1087 (1953).

39. D. R. Peacor, Z. Kristallog. **138**, 274 (1973).

40. H. D'Amour, W. Denner and H. Schltz, Acta Cryst. **B 35**, 550 (1979).

41. W. G. Wycoff, "Crystal Structures", Vol. 1, 2nd ed., John Wieley & Sons, Inc., p 313 (1968).

42. J. J. Erpenbeck and W. W. Wood, Mod. Theoret. Chem., "Stat. Mechanics," **6**, 1 (1977).

43. N. E. W. Hartley, and T. R. Wilshaw, "Deformation and Fracture of Synthetic Quartz", J. Mats. Sci., **8**, 265 (1973).

44. C. Y. Su, P. R. Skeath, I. Lindau W. E. Spicer, J. Vac. Sci. Technol. **19**, 481 (1981).

45. R. Ludeke and A. Koma, Phys. Rev. Lett. **34**, 1170 (1975).

46. J. McBride, S. Heimel, J. G. Ehlers, and S. Gordon, "Thermodynamic Properties to 6000'K for 210 Substances Involving the First 18 Elements" NASASP-3001, Washington (1963).

47. D. R. Stull and G. C. Sinke, "Thermodynamic Properties of the Elements", Advances in Chemistry. Ser., No. 18, Washington (1956).

48. "Thermodinamicheskie svoistva individual'nykh veshchestv (Thermodynamic Properties of Individual Substances)", Eds: V. P. Glushko, L. V. Gurvich, G. A. Khachkuruzov, I. V. Veits, and V. A. Medvedev, 2nd edition, 1 and 2, Izd. AN SSSR (1962).

49. E. C. Baughan, Quart. Rev., 7, 116 (1953).

50. S. G. Davis, D. F. Anthrop, and A. W. Searcy, cited in (A. W. Searcy and A. G. Tharp, J. Phys. Chem., 64, 1539 (1960)).

51. JANAF Thermochemical Tables, PB-168370, Clearinghouse, U. S. Depart. of Commerce (Nat. Bur. Stand.), Aug., 1965.

52. Feb. 20, 1975 LBL Report 3720.

53. L. Brewer, et al., Advanced High Temp. Chem., 2, 1 (1969).

54. V. P. Glushko, et al., "Thermicheskie konstanty veshchestv (Thermal Constants of Compounds)", Handbook, No. 2, VINITI AN SSSR (1965).

55. "Selected Values of Chemical Thermodynamic Properties, Pt. 1. Tables for the First Twenty-three Elements in the Standard Order of Arrangement", Eds: D. D. Wagman, W. H. Evans, J. Halow, V. B. Paker, S. M. Bailey, and R. H. Schumn, Nat. Bur. Stand., Technical Note 270-1, issued October 1, 1965.

56. W. D. Geed, J. Phys. Chem., 66, 380 (1962).

57. W. D. Good, J. L. Lacina, B. L. De Prater, and J. P. McCullough, J. Phys. Chem., 68, 579 (1964).

58. C. N. Cochran and L. M. Foster, J. Phys. Chem., 66, 380 (1962).

59. A. D. Mah, Bur. Mines Report of Investig., 5600, U.S. Dept. of Interior, Washington, 1959.

60. W. A. Roth and H. Troitzsch, Z. anorg. allg. chem., 260, 337 (1949).

61. G. L. Humphrey and E. G. King, J. Am. Chem. Soc., 74, 2041 (1952).

62. F. D. Rossini, D. D. Wagman, W. H. Evans, S. Levine, and I. Jaffe, "Selected Values of Chemical Thermodynamic Properties", Circ. Nat. Bur. Stand., 500 (1952).

63. D. D. Wagman, T. R. Muson, W. H. Ewans, and E. J. Orosen, Nat. Bur. Stand., Report 3456, Aug. 30, 1954.

64. J. P. Coughlin, "Heat and Free Energies of Formation of Inorganic Oxides. Contribution to the Data on Theoretical Metallurgy", XII, Bur. Mines Bull., 542, Washington (1954).

65. H. E. Schwiete and C. Hummel, "Forschungsber. Wirtsch. u. Verkehrsmin"., Nordrhein-Westfalen, No. 515, 1105 (1958); C. Hummel and H. E. Schwiete, Glastechn. Ber., 32, 327, 413 (1959).

66. A. F. Wright and A. J. Leadbetter, Phil. Mag., 31, 1391 (1975).

67. K. Hubner, Phys. Stat. Sol., A 40, 487 (1977).

68. J. D. Jorgensen and F. J. Rotella, J. Appl. Cryst., in Press.

69. A. F. Wells, "Crystal Chemistry", 4th ed., Oxford University Press, London, 1975, Chapt. 23.

70. D. F. Grant and E. J. Gabe, J. Appl. Cryst., 11, 114 (1978).

71. H. D. Hegaw, "Crystal Structures: A Working Approach", W. B. Saunders Co., P 453 (1973).

72. A. J. Cohen and G. G. Sumner, Am. Min., 43, 58 (1958).

73. G. A. Lager, AIP Conference Proceedings 89, Ed.: John Faber, Ju, p 75 (1981).

74. K. F. Lindman, Acta Soc. Fenn., 46 (5), 1 (1916).

Table 1 Lattice Sums for Crystalline SiO_2 Forms

	α-crist.	α-quartz	β-crist.	β-quartz
ε^m_{11}	4.0575	4.1148	4.0388	4.1048
ε^m_{12}	9722.33	9328.37	9796.98	9870.78
ε^m_{22}	41.3494	36.7629	42.0266	48.1561
ε^m_{21}	4861.17	4164.88	4898.46	4929.74
ε^n_{11}	5.2401	5.6759	5.0999	5.6325
ε^n_{12}	202.442	188.962	202.892	204.702
ε^n_{22}	19.5795	20.2410	19.3041	21.5124
ε^n_{21}	101.221	94.4946	101.444	102.302
T_{111}	5.7840	8.3242	4.94088	8.0688
T_{112}	-191.313	-117.663	-202.276	-175.685
T_{122}	174.512	195.381	167.158	195.231
T_{222}	62.0504	76.5891	57.5318	73.9876
T_{221}	174.555	195.427	167.131	195.237
T_{211}	-47.8405	-29.4278	-50.5788	-43.9041

Table 2 Cohesive Energies for Crystalline SiO_2 Forms*
(in Kcal/mole)

	calculated		experimental
	set #1	set #2	
α-c	-441.4	-435.0	-430.8+22
α-q	-436.6	-428.3	-431.2+17
β-c	-452.2	-443.7	-436.1+17
β-q	-445.2	-433.8	-436.5+15

* Experimental cohesive energies were obtained for the following reaction.

$$SiO_2(c) = Si(g) + 2\ O(g)$$

using standard enthalpies of formation for the reactants and products.(33, 46-65)

Table 3 Cross Parameters calculated from Crystalline SiO_2 Data

	set #1	set #2
$\epsilon_{(Si-O)}$, (°K)	47354.	58889.
$r_{o(Si-O)}$, (Å)	1.622	1.578
$z_{(Si-Si-O)}$, ($°K Å^{6}$)	5659026.	317513.
$z_{(Si-O-O)}$, ($°K Å^{6}$)	4485348.	7909849.

* These two sets of parameters satisfy eq.6 and eq.14 for both α-c and α-q.

Table. 4 Mean Peak Positions for RDF and ADF

type of SiO_2 form	source of data*	d_{Si-Si} (Å)	d_{O-O} (Å)	d_{Si-O} (Å)	Si-O-Si angle	O-Si-O angle	temp (°K)**
α-c	cal set #1	3.08	2.57	1.59	155	109	300
	cal set #2	3.07	2.60	1.60	147	108	300
	exp (39)(66)	3.077	2.60 ~ 2.65	1.605, 1.608	146.44	108.0 ~ 111.7	301
	exp (67)		2.58 ~ 2.63	1.60 ~ 1.61	147		298
α-q	cal set #1	3.06	2.58	1.59	146	107	300
	cal set #2	3.06	2.61	1.60	144	111	300
	exp (67)		2.60 ~ 2.67	1.60 ~ 1.61	144		298
	exp (68)	3.0577	2.616, 2.619	1.609, 1.611	143.5, 143.7	108.75	296
	exp (40)	3.058	2.60 ~ 2.67	1.616 1.620	141.87	106.5 ~ 111.6	298
	exp (69)			1.597, 1.617			298
	exp (70)			1.606, 1.612			298
	exp (71)				143.45		296
	exp (72)				143.65		298
	exp (73)					106.75, 109.32	296
	exp (74)					110.63	296
β-c	cal set #1	3.09	2.55	1.57	160	109	300
	cal set #2	3.09	2.58	1.58	155	108	300
	exp (39)	3.068	2.60 ~ 2.69	1.612	146.69	107.6, 112.8	503
	exp (67)		2.53	1.55			573
β-q	cal set #1	3.10	2.59	1.59	158	108	300
	cal set #2	3.10	2.60	1.61	151	110	300
	exp (41)	3.10	2.59 ~ 2.70	1.62	146.9	101.3 ~ 116.1	873
	exp (67)		2.60	1.63	144		873

* cal: calculated value, exp: experimental value
** temp: the temperature at which the data were obtained.

FIGURE CAPTIONS

FIGURE 1. Radial Distribution Function for α-cristobalite at $300^{o}K$. The curve is obtained from the positions of Si and O atoms averaged over 500 steps after full equilibration.

FIGURE 2. Distribution Function of $O - Si - O$ and $Si - O - Si$ angles for α-cristobalite at $300^{o}K$. The results represent averaged values over 500 steps after full equilibration.

FIGURE 3. Schematic representation of the regular (100) surface of α-cristobalite; (a) before and (b) after relaxation. The top view shows one of the periodic cells from the z-direction (perpendicular to the exposed surface). The side view shows the same cell viewed from the x-direction. During the relaxation process, only the top O atom was displaced slightly, while the rest of the system remained virtually unchanged. (Large open circles represent Si atoms, and small solid circles are O atoms.)

FIGURE 4. Schematic representation of the reconstructed O-rich (001) surface of α-cristobalite. Peroxide bridges formed by excess O atoms are responsible for the surface reconstruction. (Si and O atoms are shown in large open and small solid circles, respectively.)

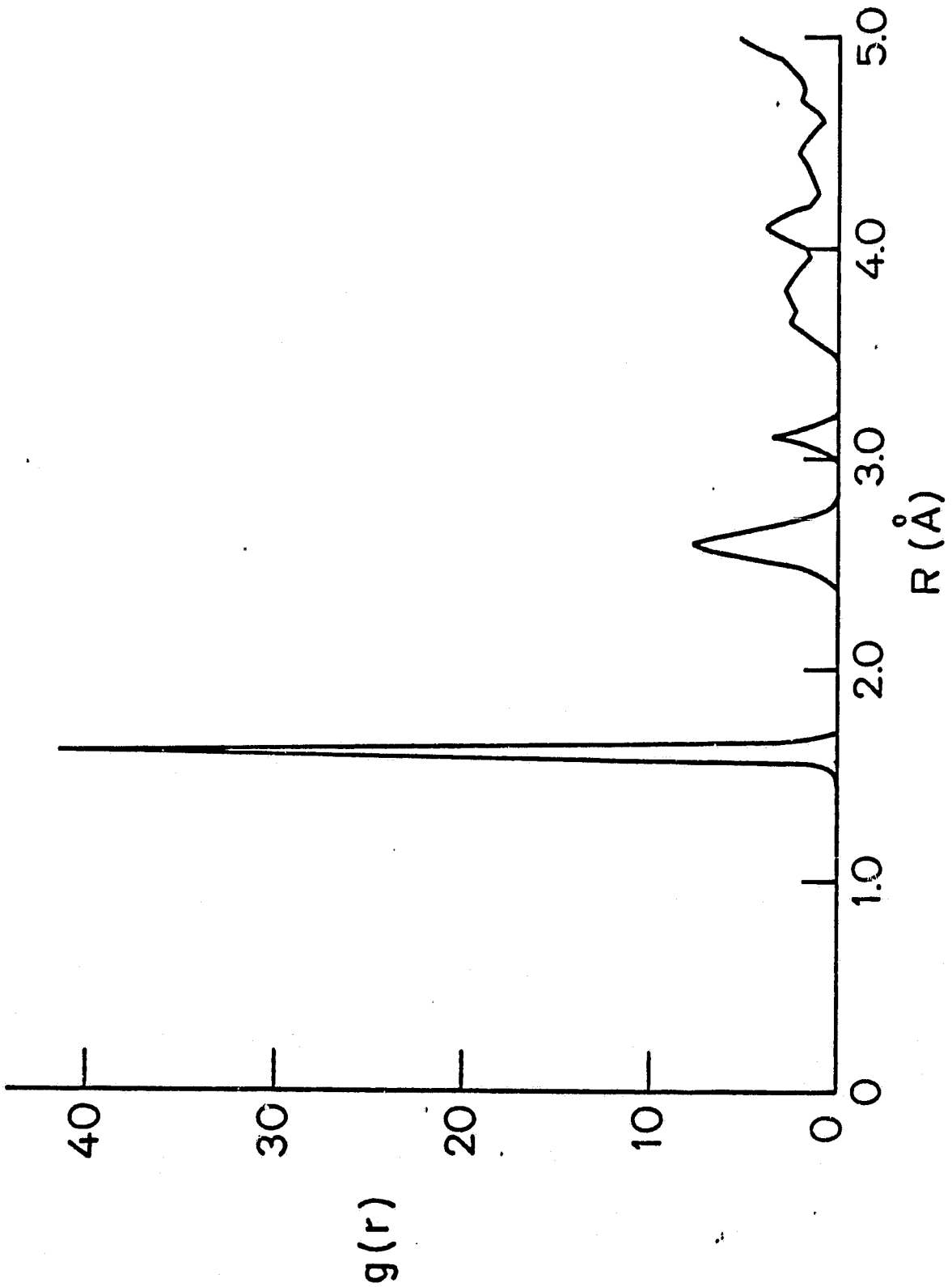

Figure 1

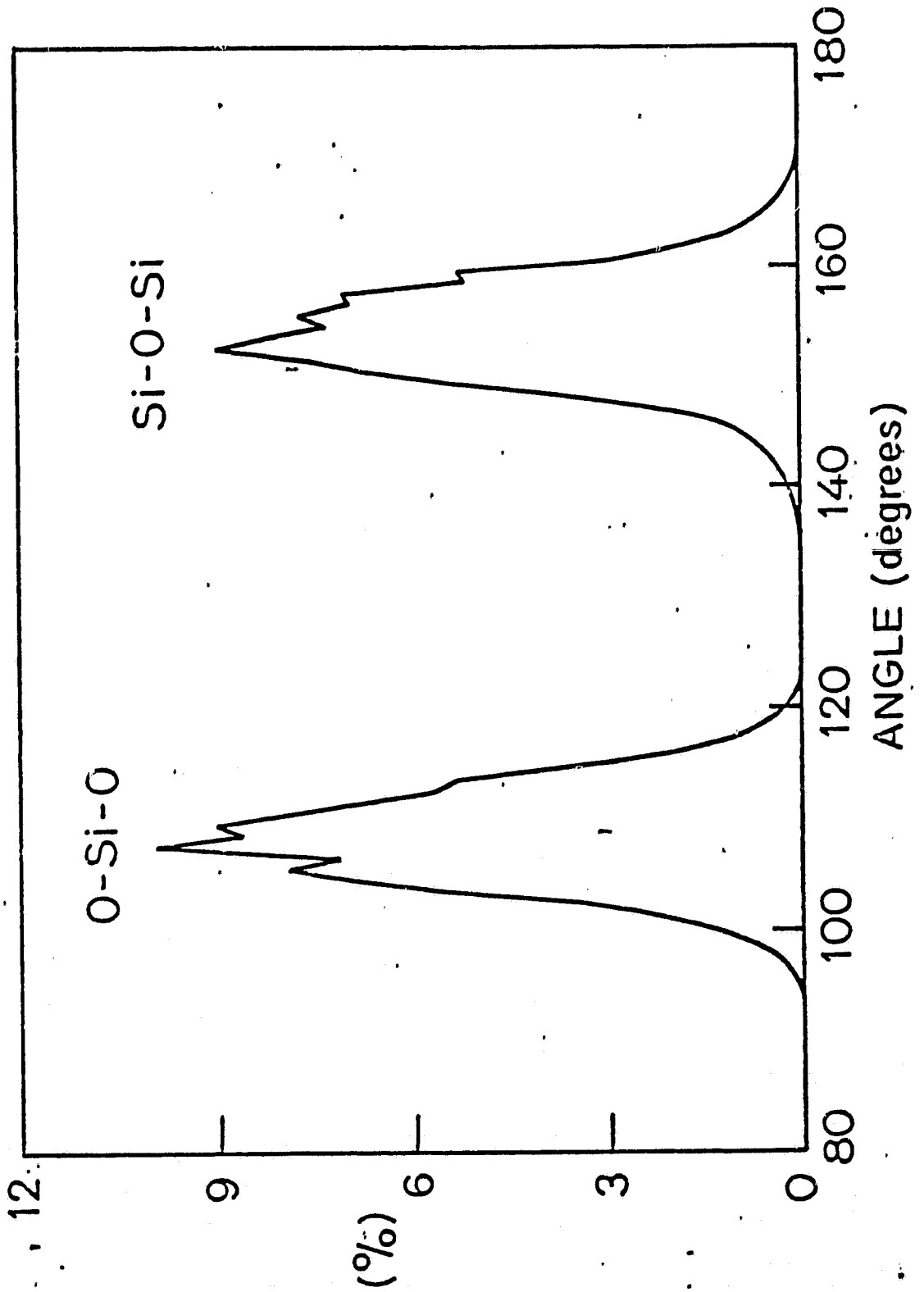

Figure 2

TOP VIEW

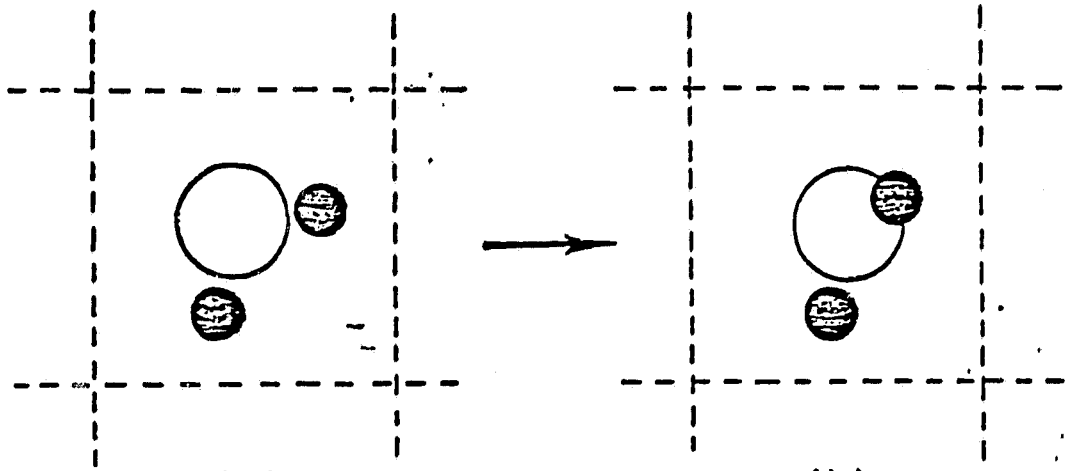

SIDE VIEW

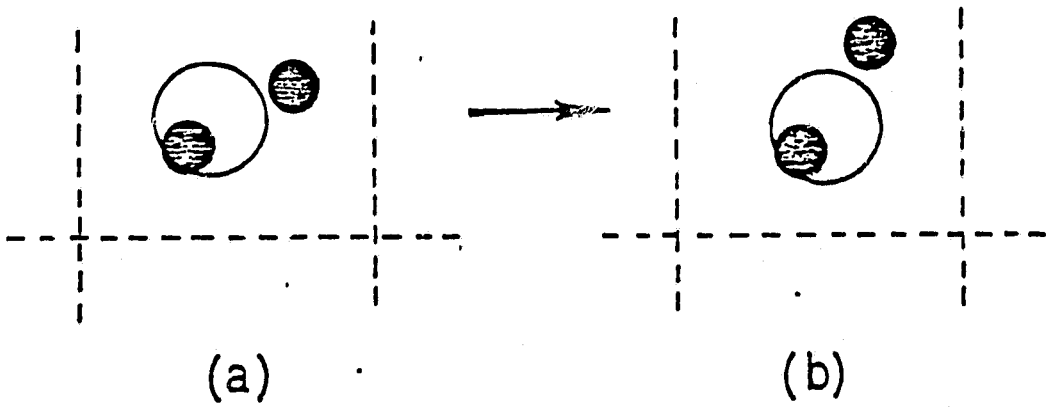

Figure 3

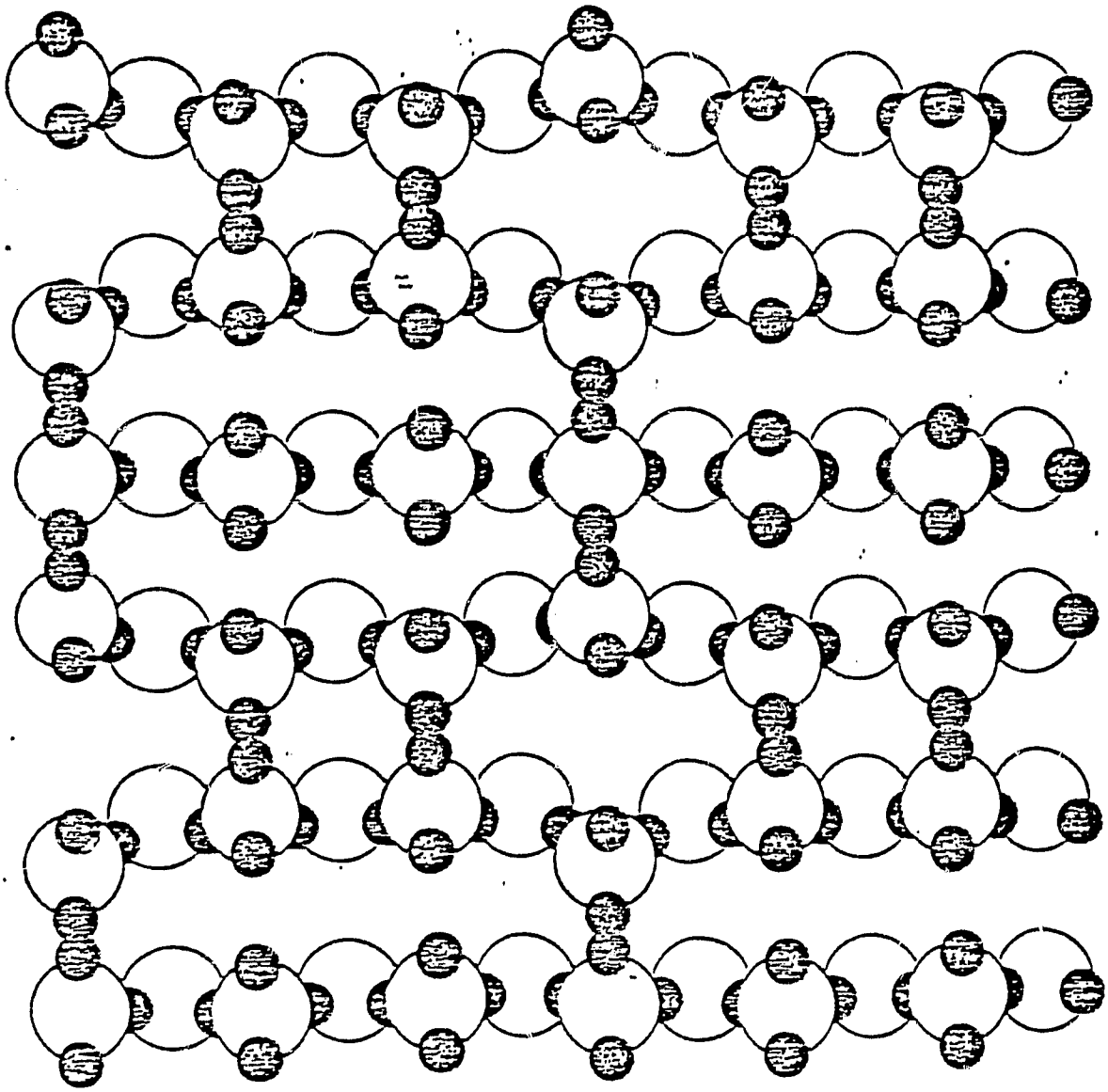

Figure 4.

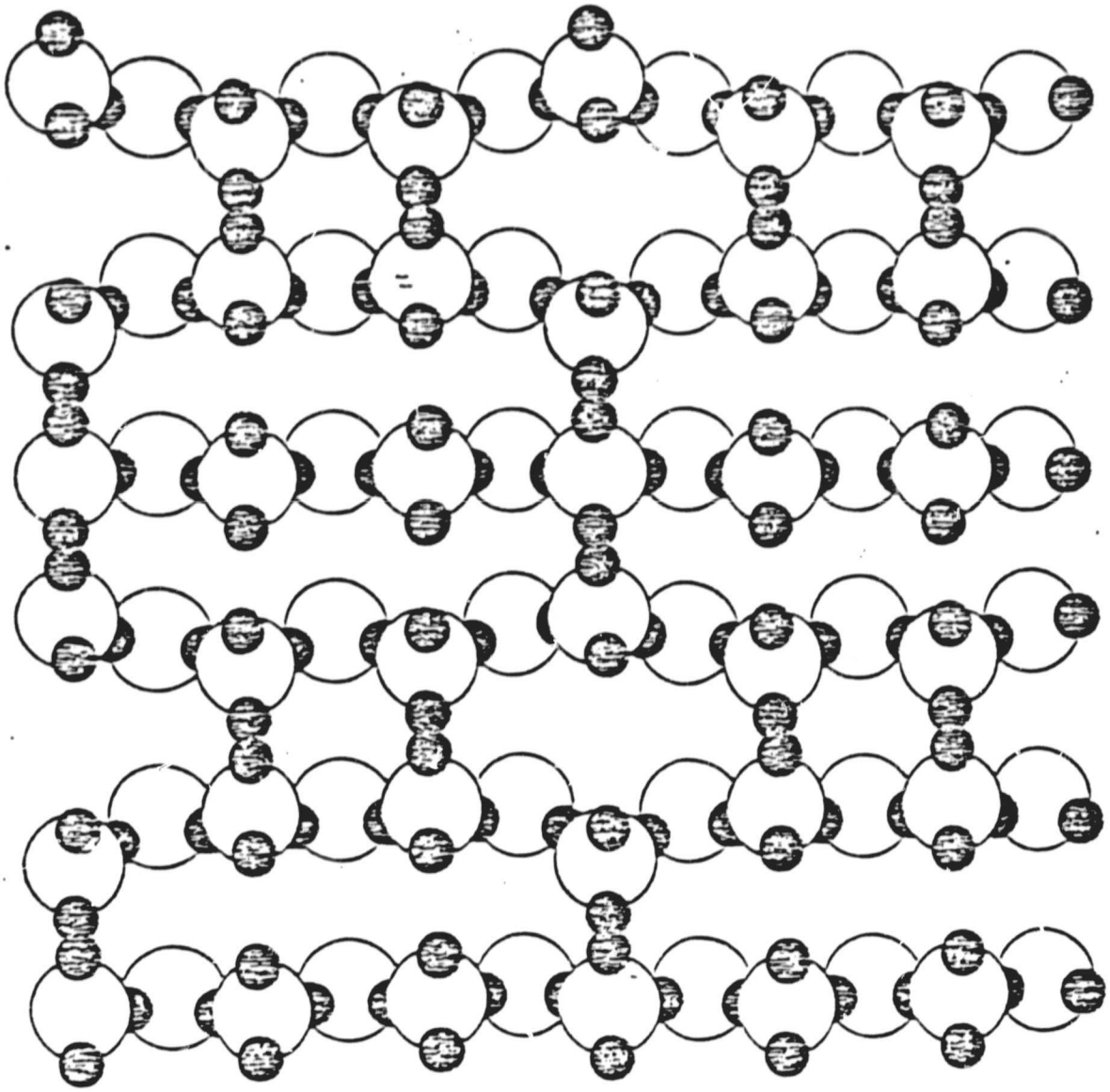

Figure 4.

CHAPTER II.

Crack propagation studies in two-dimensional triangular lattices.

PROPAGATION OF CRACKS IN 2D LATTICES

This investigation is an extension of the earlier study which had been carried out last year considering a static approach. General characteristics of the model considered in this new study are basically similar to the previous one. Again a 2D triangular lattice has been used with particles interacting via Lennard-Jones type potentials. However, in this case, the effect of the temperature was taken into account by using a molecular dynamics simulation technique. Therefore, the results are expected to be more realistic. Simulations for two-dimensional systems are relatively easier to analyze than results for three-dimensional systems. First of all, 2D systems contain a smaller number of particles and, therefore, require less computer time. Results can be represented by simple 2D plots and problems arising due to the multi-particle character of the system are easily identifiable. Thus, the analysis of the 2D system provides considerable information not only about the microscopic nature of the crack growth phenomenon, but also provides some knowledge about "how to interpret the simulation results." The question of the credibility of these 2D results, of course, remains unanswered. At this stage, it is not known how to extrapolate results obtained from a 2D simulation to a 3D domain. However, the results obtained in this study together with several other reports [1,2] in the literature indicate that 2D systems, in most cases, do exhibit characteristics similar to 3D systems.

Atomistic level analysis of the crack propagation process

using computer simulation techniques has been the subject of several earlier investigations. In the literature we could find only a few reports relevant to the study carried out in this investigation. In the report by Ashurst and Hoover [1], the fracture phenomenon was investigated based on a truncated Hook's law force. They have found that, even with this very simplistic force law, their static simulation furnished results for energy, entropy, stress concentration and crack structure all to be consistent with expectations from macroscopic elastic theory.

The other relevant and more recent study was reported by Dienes and Paskin [2]. In this modeling study they also considered a 2D triangular lattice with particles interacting via the Lennard-Jones function. A crack has been introduced in the interior of a pre-stressed sample. The crack was initiated by "cutting" the bonds between a given number of atoms at the central portion of the sample. The interatomic potential was artificially set to zero between these atoms. According to their report, the condition would correspond to the insertion of a very thin knife to create the crack. Furthermore, in the energy and force calculations, they only considered nearest neighbor interactions (by taking Rcut = 1.6 ro). In their model, the crack was aligned parallel to close-packed rows and displayed a linear path in its propagation. Finally, they found that their results are quantitatively good at the early stages of the propagation process.

The main objective of the present study is to investigate the crack propagation phenomenon at a microscopic level. For this purpose, a 2D triangular lattice was taken into consideration and the effect of a tensile load imposed on the system was analyzed.

In the following sections, first a perfect lattice, then a lattice with a surface crack under various conditions was investigated.

PERFECT LATTICE

As a perfect 2D lattice, the basal plane of an hcp lattice was taken into consideration. A system of 2400 particles in a rectangular shape (80 by 30) was first generated in static equilibrium. A tensile load was applied in the [112] direction, which is the close-packed direction. This direction was also chosen as the x-direction in our cartesian coordinate system. The load was imposed in small incremental strains (in this case elongations) of 0.01. This was performed uniformly throughout the system by factorizing all the x-components of the position vectors describing the system. In the x-direction, periodic boundary conditions (PBC) were applied to provide continuity for the system (in the tensile direction), and also to furnish two free surfaces in the y-direction. In a general sense, the imposed PBC provides the desired tensile strain on the system.

The system was relaxed after every incremental strain by a molecular dynamics code. A cut-off radius. Rcut, of 2.86 ro was considered for the energy and force calculations. This Rcut is between the fourth and fifth neighboring shells surrounding the central atom and provides 30 neighbors. The reduced time step was taken as 0.01 and the reduced temperature was $T^* = 0.02$ (to compare with real systems; e.g., for copper these represent 2.5E-15 seconds and 100 K, respectively. Additional information about the cut-off radius and the molecular dynamics program are included in

Appendix I and II. The stress-strain curve calculated as a result of this elongation-relaxation process is shown in Fig. 1 up to e = 0.88.

2D LATTICE WITH AN EXISTING CRACK

A lattice with an initial surface crack was generated by removing 9 particles from the lower surface region of a perfect lattice (see Fig. 2). This system, now with an existing surface crack, was elongated and relaxed by the molecular dynamics code in a similar way explained above for the perfect case. First, the effect of the temperature on the stress-strain curve was analyzed up to e = 0.03. Figure 3 shows two curves, dotted and solid, representing the stress-strain curves for $T^* = 0.1$ and $T^* = 0.02$, respectively. The shift in the dotted curve (high temperature curve) is mainly due to the thermal expansion. For lower strain values, these curves represent fully equilibrated systems. However, for strains higher than 0.02, systems may require additional relaxation times to equilibrate completely. The difficulty involved in attaining the equilibrium is mainly due to large fluctuations displayed by the stress values calculated as derivatives of the energy. At this stage, we believe that the general trend exhibited by these two curves is sufficiently accurate for the present investigation. Any further incremental elongations (in addition to e = 0.03) cause the crack to propagate. Determination of the critical strain; i.e., the strain at which the crack first starts to propagate, is difficult to assess. For this purpose we performed three separate runs with three different pre-strained systems, namely with e = 0.03,

e = 0.035 and e = 0.04, all at T* = 0.02. The 2D lattice with the surface crack was strained in one single step from its original length up to 3.0, 3.5 and 4.0% elongations. In the case of e = 0.03, the crack did not exhibit any growth and the overall configuration of the systems remained unchanged up to 3500 time steps. However, for both e = 0.035 and 0.04 cases, the propagation of the crack took place. In these prestrained cases, we simulated the system under nonequilibrium isothermal conditions. For the e = 0.035 case, the crack growth first initiated after 1000 iteration steps. Figure 4 displays the stages of this relaxation process up to 3200 iterations, at which the system reached almost to an equilibrium state. The darker circles in the figures represent particles with higher stresses. For the e= 0.04 case, on the other hand, the crack propagated much earlier (obviously because of the high strain imposed initially). The crack started growing first at the 500'th iteration step and the system attained an equilibrium state at approximately 2400 iteration. The stages of this propagation process are shown in Fig. 5. Again, the darker circles display particles with higher stresses. In both cases, the particles at the crack tip exhibited high stresses consistently. Furthermore, the crack propagated along the close-packed rows of the lattice and, at the same time, tried to remain perpendicular to the applied load by choosing a zig zag path. These behaviors are very much consistent with experiments and theories based on macroscopic considerations and, therefore, indicate the adequacy of the present atomistic level simulation procedure. The relaxation of the system can be

followed in Fig. 6 where the average stress is plotted versus the iteration steps. The oscillatory behavior of this curve is a temperature effect mainly due to vibrational motions displayed by individual particles in the system. From the snapshots shown in Fig. 5, we also calculated the velocity of the crack propagation. The curve in Fig. 7 represents the variation in the crack propagation velocity as a function of the calculated average stress. The upper range of this curve is near the velocity of sound propagation. This is expected according to a report by Ashurst and Hoover [1].

REFERENCES

1. W. T. Ashurst and W. G. Hoover, Phys. Rev. B 14, 1465 (1976).
2. G. J. Dienes and A. Paskin, in "Atomistics of Fracture," ed: R. M. Latanision and J. R. Pickens (Plenum Press, New York, 1983) p 671.
3. P. O. Esbjorn and E. J. Jensen, J. Phys. Chem. Solids 37, 1081 (1976).

APPENDIX I

Many of the characteristics of a 2D Lennard-Jones lattice are known [3]. Here, the energy and its derivatives of a 2D triangular lattice will be formulated. For a perfect lattice, with particles interacting via two-body central potentials, the total interaction energy of the bulk system can be expressed as;

$$\Phi = \frac{N}{2}\sum_{i}^{N} u(r_i) \tag{1}$$

where, N is the total number of particles in the system, and $u(r_i)$ represents the pair potential function between two particles in the system separated by a distance r_i. For the Lennard-Jones case we have;

$$u(r_i) = \epsilon\left((\frac{r_o}{r_i})^{12} - (\frac{r_o}{r_i})^{6}\right) \tag{2}$$

with ϵ and r_o denoting the energy and the internuclear distance at the equilibrium, respectively. The stability criterion for a 2D system, in the absence of an external force, is given by;

$$\frac{\partial \Phi}{\partial \mathcal{A}} = 0 \tag{3}$$

where, $\mathcal{A}$ is the total area occupied by the system. For a system of N particles we have:

$$\mathcal{A} = Na_o \tag{4}$$

with a_o denoting the area per particle. For a triangular lattice a_o is equal to $\sqrt{0.75}d^2$ where d denotes the nearest neighbor distance. Considering lattice sum notations, from equations 1 and 2 we obtain:

$$\Phi = \frac{N\epsilon}{2}\left(B_{12}(\frac{r_o}{d})^{12} - 2B_6(\frac{r_o}{d})^{6}\right) \tag{5}$$

where,

$$B_{12} = \sum_{i}^{N}(\frac{d}{r_i})^{12} \tag{6a}$$

and

$$B_6 = \sum_{i}^{N}(\frac{d}{r_i})^{6} \tag{6b}$$

APPENDIX I

Many of the characteristics of a 2D Lennard-Jones lattice are known [3]. Here, the energy and its derivatives of a 2D triangular lattice will be formulated. For a perfect lattice, with particles interacting via two-body central potentials, the total interaction energy of the bulk system can be expressed as;

$$\Phi = \frac{N}{2}\sum_{i}^{N} u(r_i) \tag{1}$$

where, N is the total number of particles in the system, and $u(r_i)$ represents the pair potential function between two particles in the system separated by a distance r_i. For the Lennard-Jones case we have;

$$u(r_i) = \epsilon\left((\frac{r_o}{r_i})^{12} - (\frac{r_o}{r_i})^{6}\right) \tag{2}$$

with ϵ and r_o denoting the energy and the internuclear distance at the equilibrium, respectively. The stability criterion for a 2D system, in the absence of an external force, is given by;

$$\frac{\partial \Phi}{\partial \mathcal{A}} = 0 \tag{3}$$

where, $\mathcal{A}$ is the total area occupied by the system. For a system of N particles we have:

$$\mathcal{A} = Na_o \tag{4}$$

with a_o denoting the area per particle. For a triangular lattice a_o is equal to $\sqrt{0.75}d^2$ where d denotes the nearest neighbor distance. Considering lattice sum notations, from equations 1 and 2 we obtain:

$$\Phi = \frac{N\epsilon}{2}\left(B_{12}(\frac{r_o}{d})^{12} - 2B_6(\frac{r_o}{d})^{6}\right) \tag{5}$$

where,

$$B_{12} = \sum_{i}^{N}(\frac{d}{r_i})^{12} \tag{6a}$$

and

$$B_6 = \sum_{i}^{N}(\frac{d}{r_i})^{6} \tag{6b}$$

are the 2D lattice sums. Now, the condition for the minimum energy expressed by equation 3 gives:

$$\frac{r_o}{d} = (\frac{B_6}{B_{12}})^{1/6} \tag{7}$$

The definition of the equilibrium condition based on this equation is very important for calculating the nearest neihgbor distance d with respect to the equilibrium distance r_o of equation 2. The value of r_o/d depends on the total number of particles included in the summations of equation 6. A consideration of a finite cut-off radius, R_{cut}, in the lattice sum calculations, therefore, would affect the values of r_o/d as well as Φ Accordingly, R_{cut} becomes a part of the potential function, in particular, for smaller cut-off radii.

In the computer simulation studies the stress and the elastic constants are calculated at the atomistic level for every individual particle. The Lagrange strain parameters, $e_{\alpha\beta}$, for a 2D lattice may be expressed as;

$$r_i^2 = x_i^2 + 2e_{xx}x_i^2 + 2e_{yy}y_i^2 + 2e_{xy}x_iy_i + 2e_{yx}y_ix_i \tag{8}$$

The stress, for example, in the x-direction is given by:

$$\sigma_{xx} = \frac{1}{A}\frac{\partial \Phi}{\partial e_{xx}}$$

or,

$$\sigma_{xx} = \frac{6\epsilon}{a_o}\sum_i^N \left[(\frac{r_o}{r_i})^{12} - (\frac{r_o}{r_i})^6\right]\left(\frac{x_i}{r_i}\right)^2 \tag{9}$$

Similarly, for the y-direction we have:

$$\sigma_{yy} = \frac{6\epsilon}{a_o}\sum_i^N \left[(\frac{r_o}{r_i})^{12} - (\frac{r_o}{r_i})^6\right]\left(\frac{y_i}{r_i}\right)^2 \tag{10}$$

The elastic constants, $C_{\alpha\beta\gamma\delta}$, of a 2D triangular lattice have already been calculated by Esbjorn and Jensen [3], and following relations have been obtained:

$$C_{xxxx} = C_{yyyy} = 3C_{xxyy} \tag{11a}$$

and

$$C_{xxxy} = C_{yyyx} = 0. \tag{11b}$$

where,

$$C_{xxxx} = \frac{12\epsilon}{a_o} \sum_{i}^{N} \left[7\left(\frac{r_o}{r_i}\right)^{12} - 4\left(\frac{r_o}{r_i}\right)^{6} \right] \left(\frac{x_i}{r_i}\right)^4 \qquad (12)$$

As it was stated above for r_o/d and Φ cases the values of $\sigma_{\alpha\beta}$ and $C_{\alpha\beta\gamma\delta}$ are also dependent on the cut-off radius considered in the summations. Of course, for a system at the equilibrium (i.e., in the absence of external forces and if the condition described by equation 3 is satisfied) the stress components $e_{\alpha\beta}$ should be equal to zero. In investigating the effect of R_{cut}, it is very helpful to analyze the system in terms of neighboring shells. Table 1 gives these neighboring shell distances and the occupation numbers. Table 2, on the other hand, tabulates calculated values for the lattice sums, r_o/d, Φ and C_{xxxx} upto 20'th shell.

APPENDIX II.

COMPUTER SOFTWARE (TENST)

This package has been prepared mainly for investigating behaviors of two or three-dimensional monatomic systems under tensile loads. Simulations are based on a molecular dynamics technique which uses a Nordsieck-Gear algorithm. The program was prepared in a vectorized form for the Cray usage. It can handle sytems containing up to 10000 particles within reasonable computation time. The result of the calculations for positions and individual stresses can be stored for any desired intervals for further analysis. This program has also a graphics option for trajectory plots. If desired trajectories of every moving particle can be plotted for a visual inspection.

INPUT DATA AND THE DEFINITION OF PARAMETERS

(i) I/O data:

1) TITLE (Title card up to 80 characters)

2) XTIME,NRUN,NCONT,NEW,IPSTEP,XMIN,XMAX

3) IFREQ,IMEAN,ISTRES

4) NSTEP,NMEAN,IPDATE,NSBSV,NSBTS,NFINTS

5) XELO,NELO,JDIM

6) TEMP,DT,RCUT

7) EP,RO,AMASS,MOVE,FAC,LAYER

.....

x repeat LAYER times

8) W(J,K),NOO(J,K),ISQUAR

.....

9) PP(1), PP(2), PP(3), FACPBC

(ii) Definition of parameters:

TITLE= Title card up to 80 characters.

XTIME= Time limit for internal check. It should be less than the time allocated for the program run for normal termination.

NRUN= Maximum number of steps for the run.

NCONT= 1 For initial runs.

NCONT= 2 For continuation runs.

NEW= 0

IPSTEP= Trajectory plotting routine will be called in every IPSTEP times. If IPSTEP=0 no plot calls will be made.

XMIN, XMAX :Minimum and maximum points on the plot (even if IPSTEP=0 XMIN and XMAX must be defined).

IFREQ, IMEAN : In every IFREQ steps, averages of the individual stresses will be calculated for the last IMEAN steps. Always IMEAN.LE.IFREQ should be satisfied.

ISTRES= 1 Averages for stresses will be taken.

ISTRES= 0 No stress calculations will be performed.

NSTEP = Step number at the start (usually NSTEP=0). It has no effect if NCONT=2.

NMEAN= Number of steps averages to be taken. This is for the periodic printnig only.

IPDATE= Number of steps between neighbor list update.

NSBSV= Number of steps between savings of variables (coordinates and averaged values).

NSBTS= Number of steps between temperature scalings.

NFINTS= Number of step at which temperature scaling will be turned off.

XELO= Elongation factor to be multiplied by the x component of the positions for incremental elongation. (If XELO=1 no elongation will be imposed).

NELO= Number of steps between elongations

JDIM= Dimensionality of the system. (For a two-dimensional system JDIM=2).

TEMP= Temperature (in deg. Kelvin).

DT= Time steps in seconds.

RCUT= Cut-off radius (in $\AA$)

EP= Energy parameter, epsilon (in deg.)

RO= Equilibrium distance for two-body interaction (in $\AA$).

AMASS= Atomic mass (in atom gram).

MOVE= Number of mobile particles. (In general MOVE should be equal to the total number of particles).

FAC= Factor used in generating lattice points.

LAYER= Number of input files required for lattice generation.

W(J,K)= First three describe the coordinates of the original atom. Following three are the unit cell dimensions.

NOO(J,K)=Number of particles to be generated in x,y and z directions.

ISQUAR= 2 Takes square root of the W(J,K) values before the lattice is generated. If ISQUAR.NE.2 no action will be taken.

PP(1)= Length of the periodic box in the x-direction. This is for the PBC option and must be consistent with the genereted lattice coordinates.

PP(2)= 0.

PP(3)= 0.
FACPBC= Factor for PP(1) to provide the correct length for PBC.

TABLE CAPTIONS

1. Neighboring shells, number of particles in every shell, total number of particles, the distance squared and distances of shells from a central particle are given for a two-dimensional triangular lattice.

2. For every shell the values of lattice sums (B_6 and B_{12}, r_c/d, total potential energy Φ and the elastic constant C_{xxxx} are tabulated for a two-dimensional lattice (see Appendix I).

Table 1.

Shell	No. of atom in the shell	Total no. of atoms	Distance square R^2	Distance R
1	6	6	1.00000000	1.00000000
2	6	12	3.00000000	1.73205081
3	6	18	4.00000000	2.00000000
4	12	30	7.00000000	2.64575131
5	6	36	9.00000000	3.00000000
6	6	42	12.00000000	3.46410162
7	12	54	13.00000000	3.60555128
8	6	60	16.00000000	4.00000000
9	12	72	19.00000000	4.35889894
10	12	84	21.00000000	4.58257569
11	6	90	25.00000000	5.00000000
12	6	96	27.00000000	5.19615242
13	12	108	28.00000000	5.29150262
14	12	120	31.00000000	5.56776436
15	6	126	36.00000000	6.00000000
16	12	138	37.00000000	6.08276253
17	12	150	39.00000000	6.24499800
18	12	162	43.00000000	6.55743852
19	6	168	43.00000000	6.92820323
20	18	186	49.00000000	7.00000000
21	12	198	52.00000000	7.21110255
22	12	210	57.00000000	7.54983444
23	12	222	61.00000000	7.81024968
24	12	234	63.00000000	7.93725393
25	6	240	64.00000000	8.00000000
26	12	252	67.00000000	8.18535277
27	12	264	73.00000000	8.54400375
28	6	270	75.00000000	8.66025404
29	12	282	76.00000000	8.71779789
30	12	294	79.00000000	8.88819442
31	6	300	81.00000000	9.00000000
32	12	312	84.00000000	9.16515139
33	24	336	91.00000000	9.53939201
34	12	348	93.00000000	9.64365076
35	12	360	97.00000000	9.84885780
36	6	366	100.00000000	10.00000000
37	12	378	103.00000000	10.14889157
38	6	384	108.00000000	10.39230485
39	12	396	109.00000000	10.44030651
40	12	408	111.00000000	10.53565375
41	12	420	112.00000000	10.58300524
42	12	432	117.00000000	10.81665383
43	6	438	121.00000000	11.00000000
44	12	450	124.00000000	11.13552873
45	12	462	127.00000000	11.26942767
46	12	474	129.00000000	11.35781669
47	24	498	133.00000000	11.53256259
48	12	510	139.00000000	11.78982612
49	6	516	144.00000000	12.00000000
50	18	534	147.00000000	12.12435565
51	12	546	148.00000000	12.16552506
52	12	558	151.00000000	12.28820573
53	12	570	156.00000000	12.49999600
54	12	582	157.00000000	12.52996409
55	12	594	163.00000000	12.76714533
56	18	612	169.00000000	13.00000000
57	12	624	171.00000000	13.07669683
58	12	636	172.00000000	13.11487705
59	12	648	175.00000000	13.22875656

Table 2.

shell	total no. of atoms	B_6	B_{12}	r_o/d	Φ	d/r_o	$a_o C_{yxxx}$	C_{xxxx}
1	6	6.ØØØØØØØØ	6.ØØØØØØØØ	1.ØØØØØØØØ	-3.ØØØØØØØØ	1.ØØØØØØØØ	6.62941563	91.85987750
2	12	6.22222222	6.ØØ823Ø45	1.ØØ584985	-3.22191781	Ø.99418417	7.11930ØØ7	99.8Ø545Ø94
3	18	6.31597222	6.ØØ969530	1.ØØ831ØØ2	-3.31092ØØ9	Ø.99174961	7.33367ØØ7	1Ø3.316Ø7568
4	3Ø	6.35Ø95764	6.ØØ979729	1.ØØ92449Ø	-3.35574230	Ø.99Ø83978	7.41495334	1Ø4.65311688
5	36	6.35918810	6.ØØ980058	1.ØØ946246	-3.36443937	Ø.99Ø62624	7.43417132	1Ø4.96959535
6	42	6.36266Ø32	6.ØØ981Ø59	1.ØØ955424	-3.36811333	Ø.99Ø53618	7.44228Ø65	1Ø5.1Ø32Ø891
7	54	6.36812231	6.ØØ981308	1.ØØ969856	-3.3738971Ø	Ø.99Ø39459	7.455Ø5485	1Ø5.31371542
8	6Ø	6.36958716	6.ØØ981344	1.ØØ973726	-3.37544925	Ø.99Ø35664	7.45848469	1Ø5.37Ø243Ø2
9	72	6.37133668	6.ØØ981369	1.ØØ978347	-3.37730362	Ø.99Ø31132	7.46257827	1Ø5.43772555
1Ø	84	6.37263244	6.ØØ981383	1.ØØ981769	-3.37867739	Ø.99Ø27776	7.46561292	1Ø5.48775Ø99
11	9Ø	6.373Ø1644	6.ØØ981386	1.ØØ982783	-3.379Ø8457	Ø.99Ø26781	7.46651268	1Ø5.5Ø258329
12	96	6.37332127	6.ØØ981387	1.ØØ983588	-3.3794Ø782	Ø.99Ø25992	7.46722617	1Ø5.51434726
13	1Ø8	6.37386792	6.ØØ98139Ø	1.ØØ985Ø32	-3.37998754	Ø.99Ø24577	7.4685Ø618	1Ø5.53545117
14	12Ø	6.37427Ø72	6.ØØ981391	1.ØØ986Ø95	-3.38Ø41476	Ø.99Ø23534	7.46944999	1Ø5.551Ø1116
15	126	6.37439933	6.ØØ981391	1.ØØ986435	-3.38Ø55116	Ø.99Ø232Ø1	7.46975139	1Ø5.55598Ø16
16	138	6.37463623	6.ØØ981392	1.ØØ987Ø6Ø	-3.38Ø8Ø244	Ø.99Ø22587	7.47Ø3Ø6Ø7	1Ø5.56512605
17	15Ø	6.37483853	6.ØØ981392	1.ØØ987594	-3.381Ø17Ø1	Ø.99Ø22Ø64	7.47Ø77993	1Ø5.57293Ø04
18	162	6.37498946	6.ØØ981392	1.ØØ987993	-3.38117711	Ø.99Ø21673	7.47113364	1Ø5.57877Ø72
19	168	6.375Ø4371	6.ØØ981392	1.ØØ988136	-3.38123466	Ø.99Ø21532	7.47126Ø67	1Ø5.58Ø86532
2Ø	186	6.37519671	6.ØØ981393	1.ØØ988540	-3.38139696	Ø.99Ø21136	7.47161Ø08	1Ø5.58677407

FIGURE CAPTIONS

1. Stress-strain curve for a perfect 2D triangular lattice. Stress values indicate average stresses calculated for the system (in reduced units).
2. A system with a preexisting surface crack at equilibrium.
3. Temperature effect on the stress-strain curve for a system containing a surface crack. Solid and dotted lines represent $T^* = 0.02$ and $T^* = 0.1$ cases, respectively.
4. Stages of the crack propagation for a system with a surface crack pre-strained for e = 0.035. Darker circles represent particles with higher stresses. Numbers at the right side of snapshots are the iteration steps.
5. Stages of the crack propagation for e = 0.04. See caption for Fig. 4.
6. Variation in the average stress as a function of the iteration steps. For the e = 0.04 case.
7. Crack propagation velocity versus the average stress. (Units for the velocity are calculated for copper.)

STRESS-STRAIN CURVE

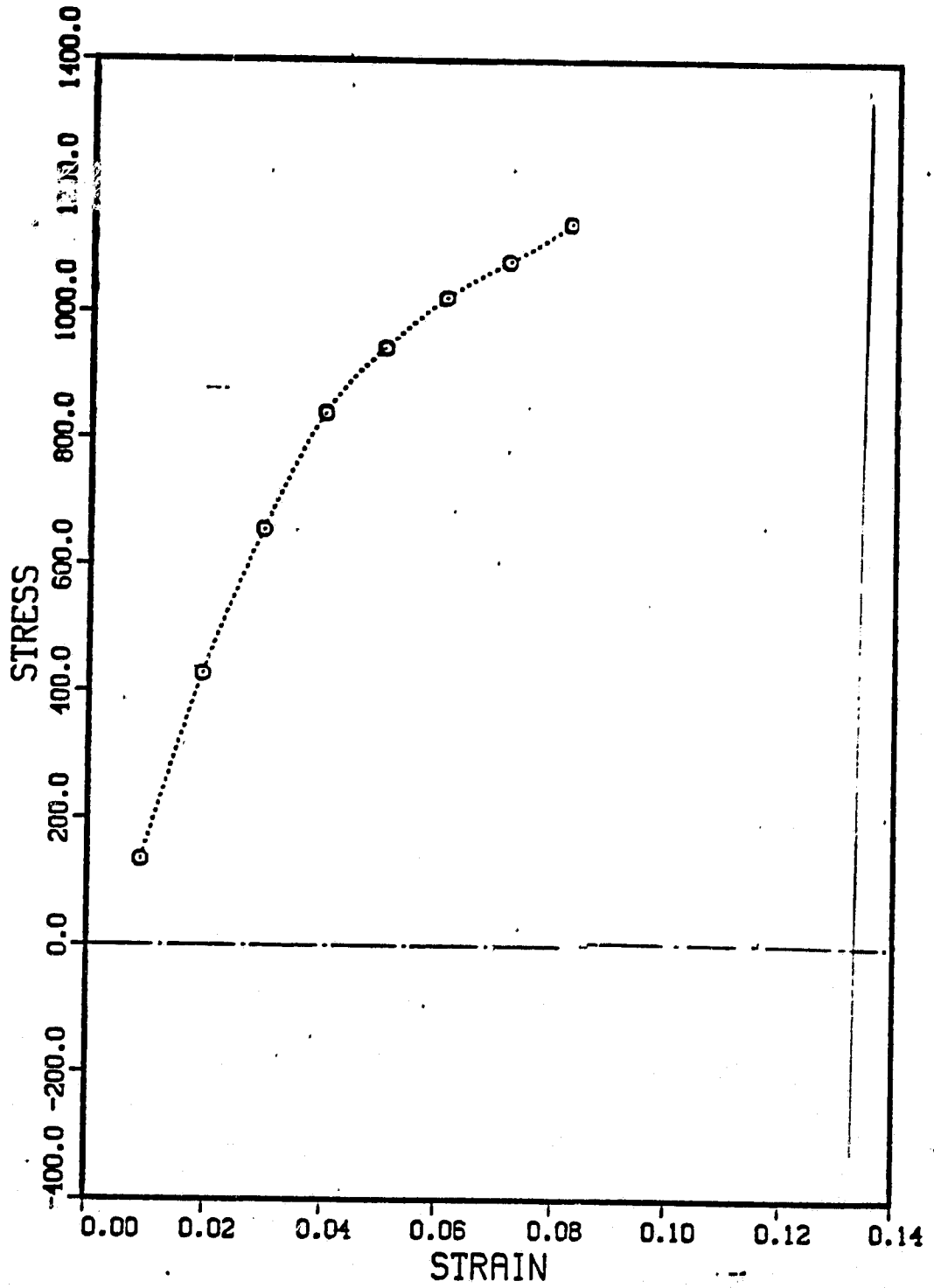

Figure 1.

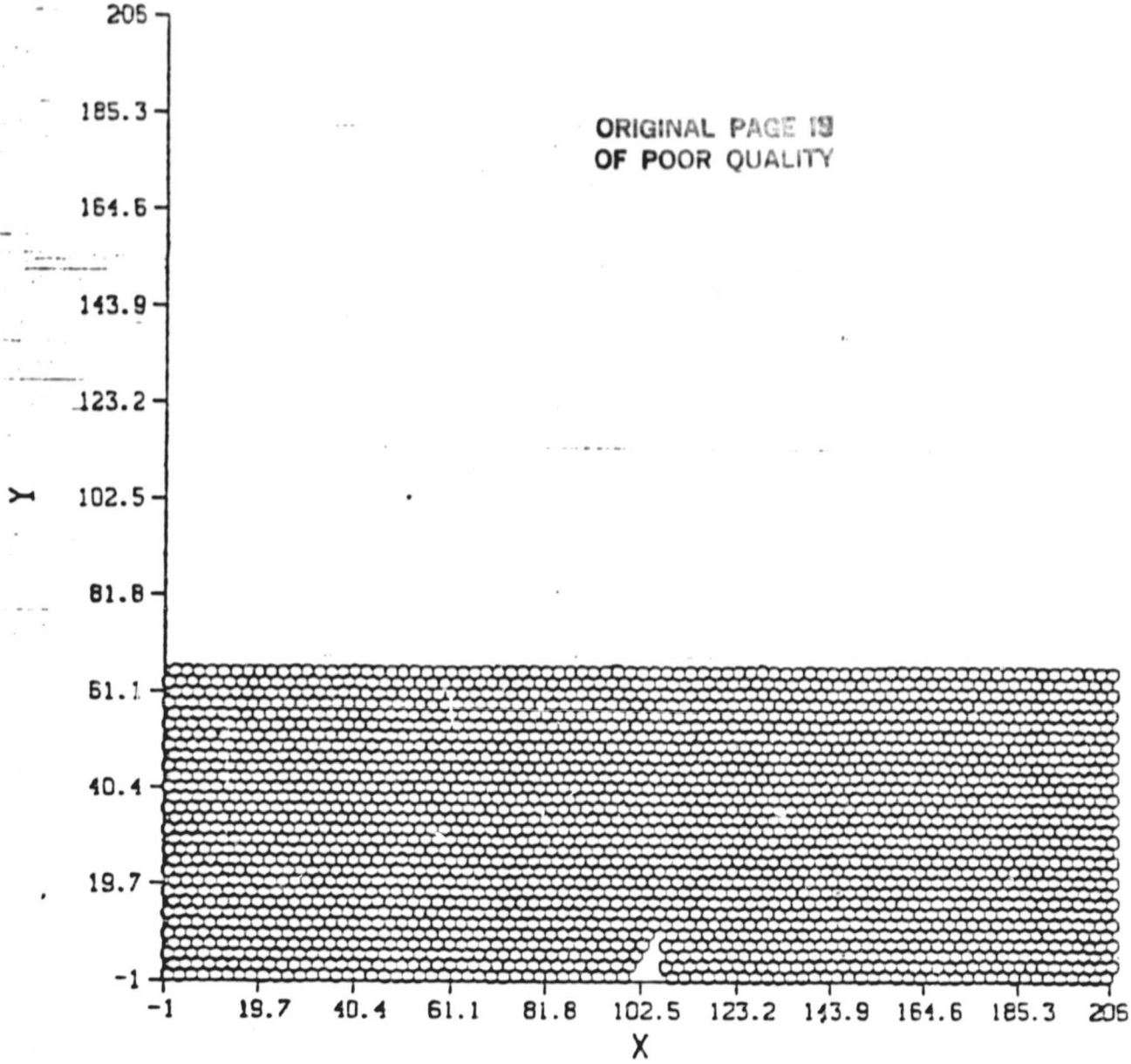

o - -.68 TO .32 2391 PTS

STEP= 100

Figure 2.

TEMPERATURE EFFECT ON THE STRESS-STRAIN CURVE

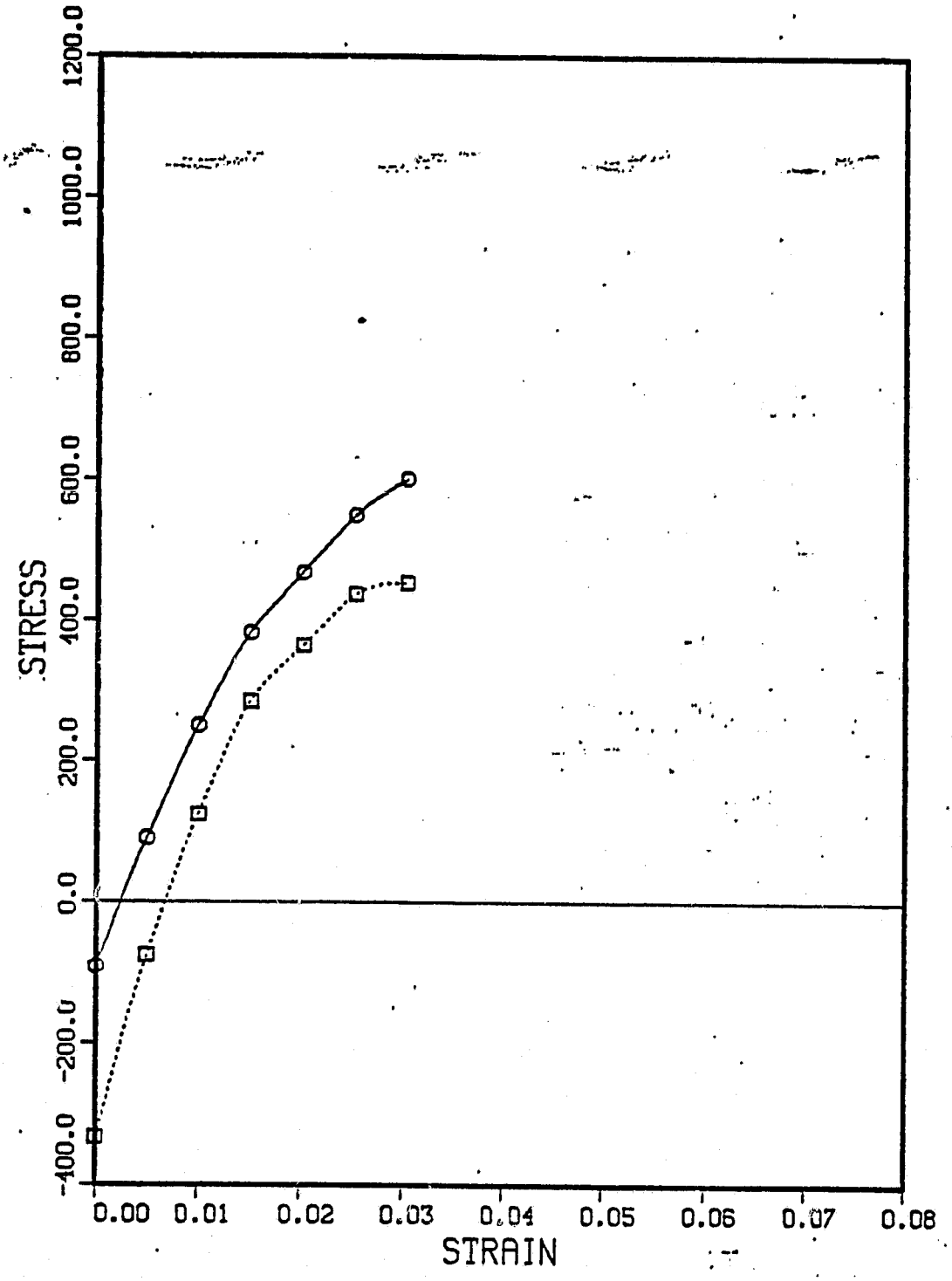

Figure 3.

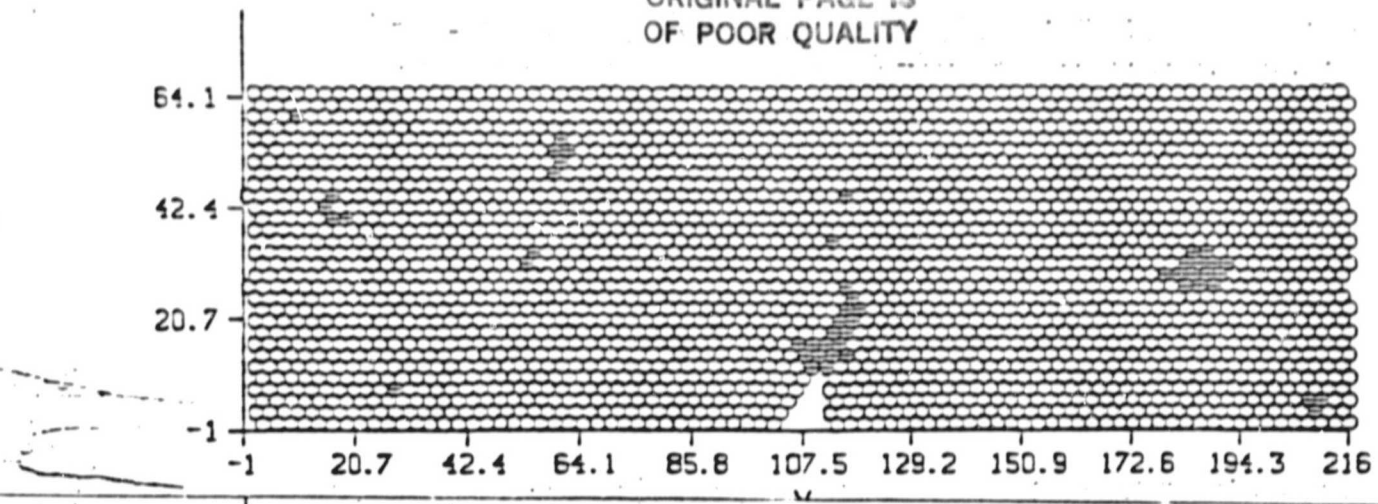

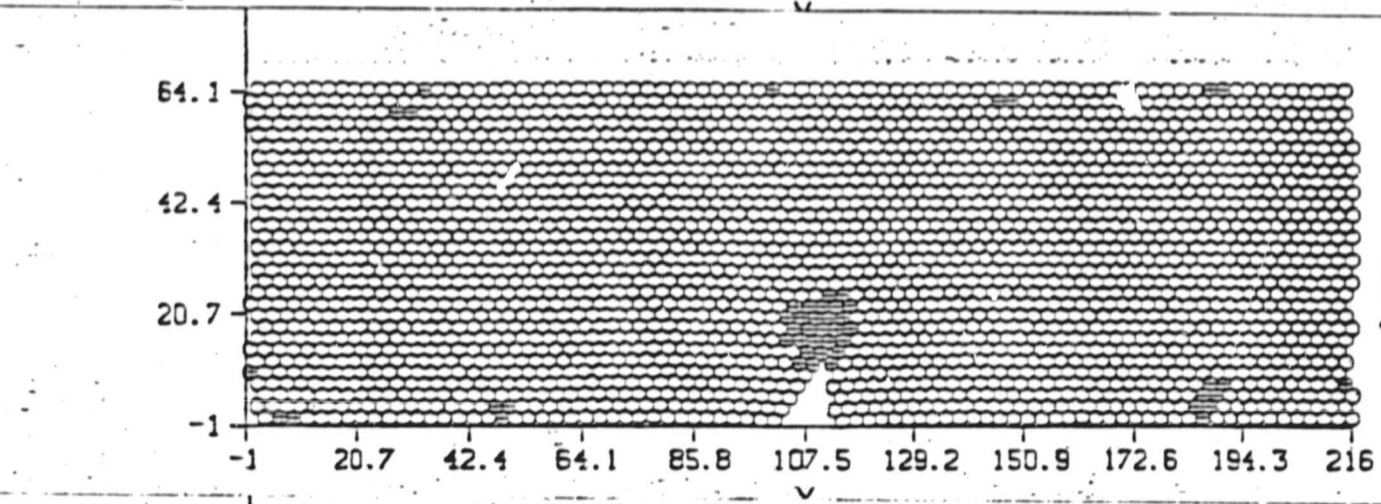

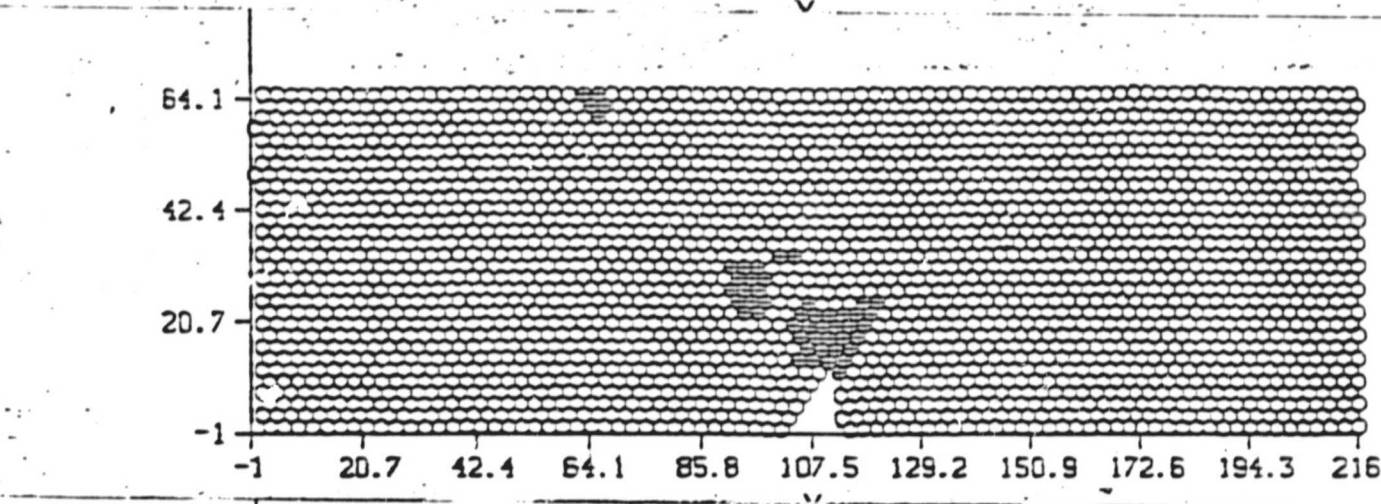

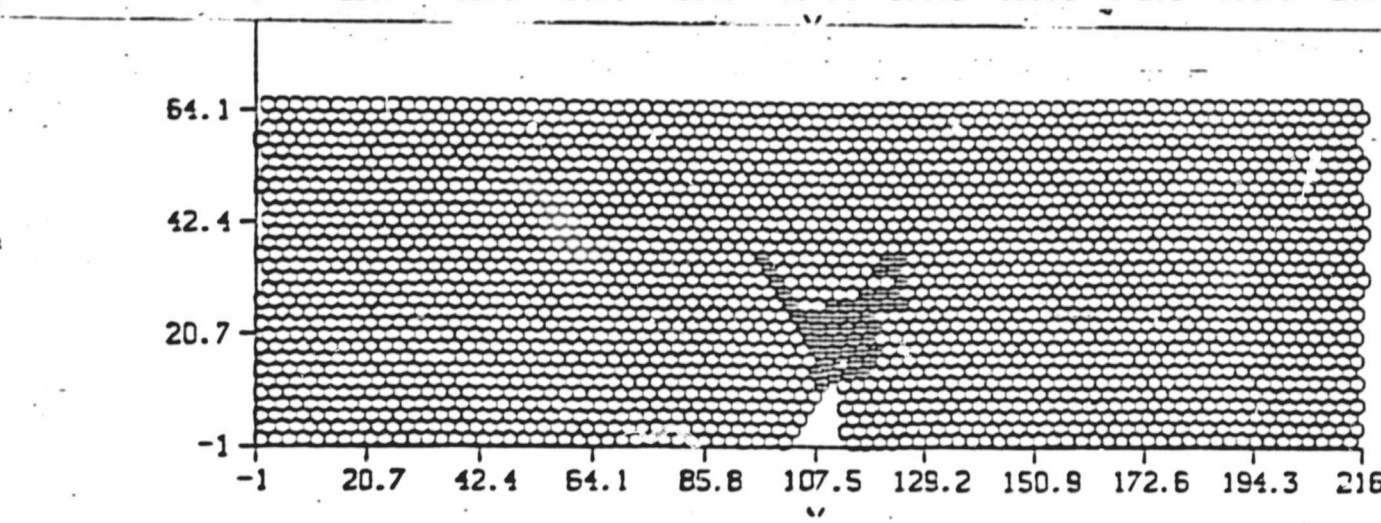

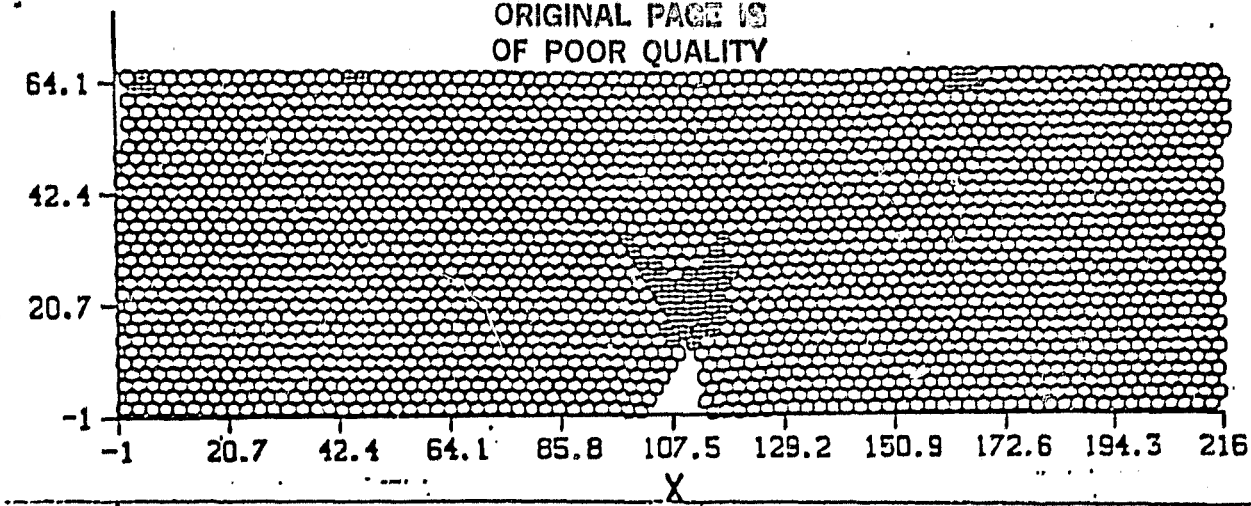

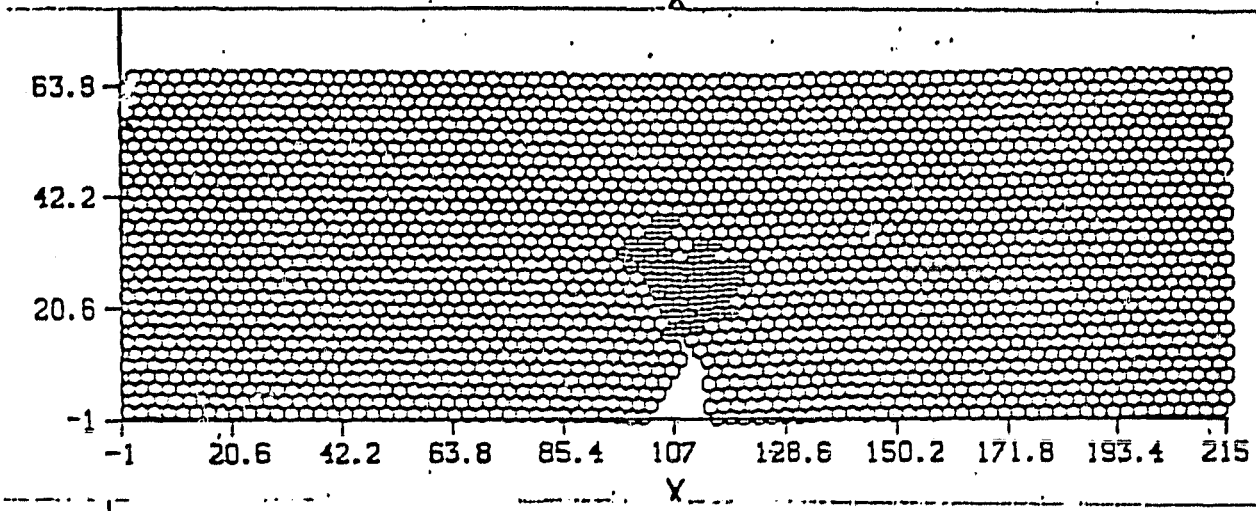

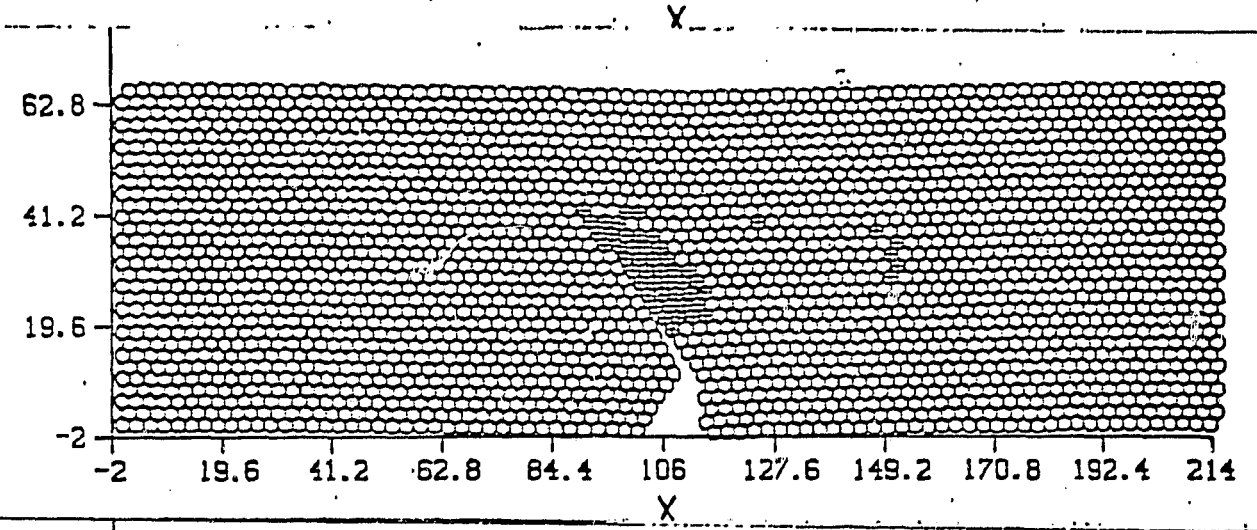

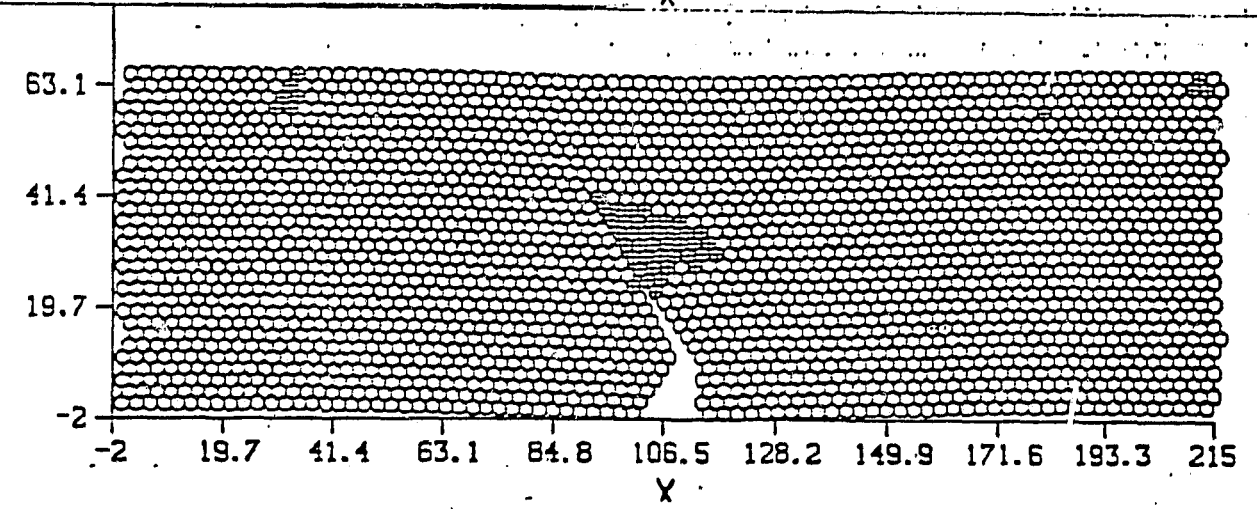

Figure 4 (cont.)

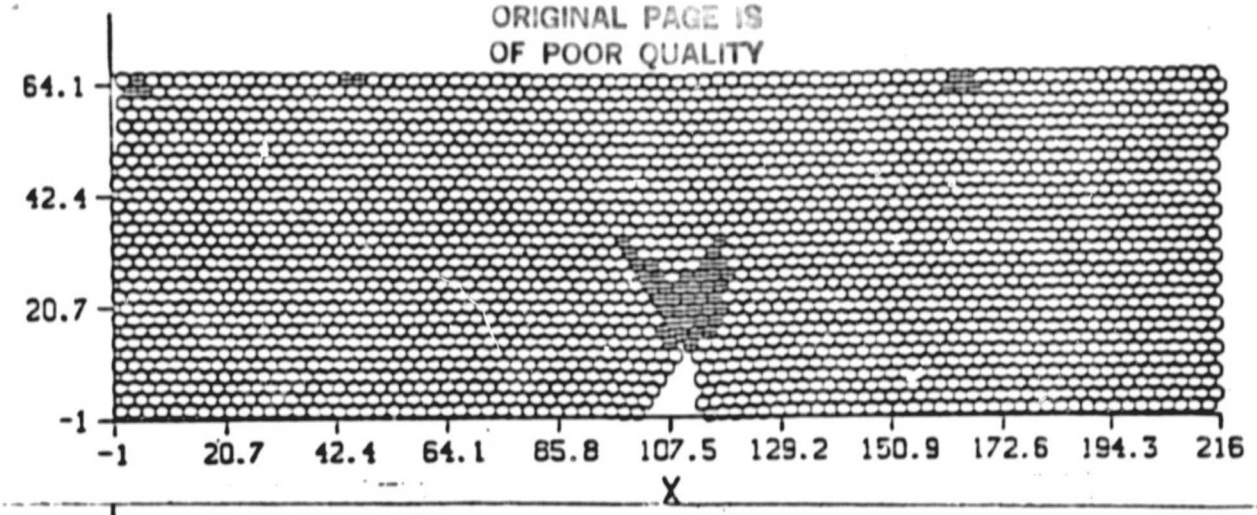

1200

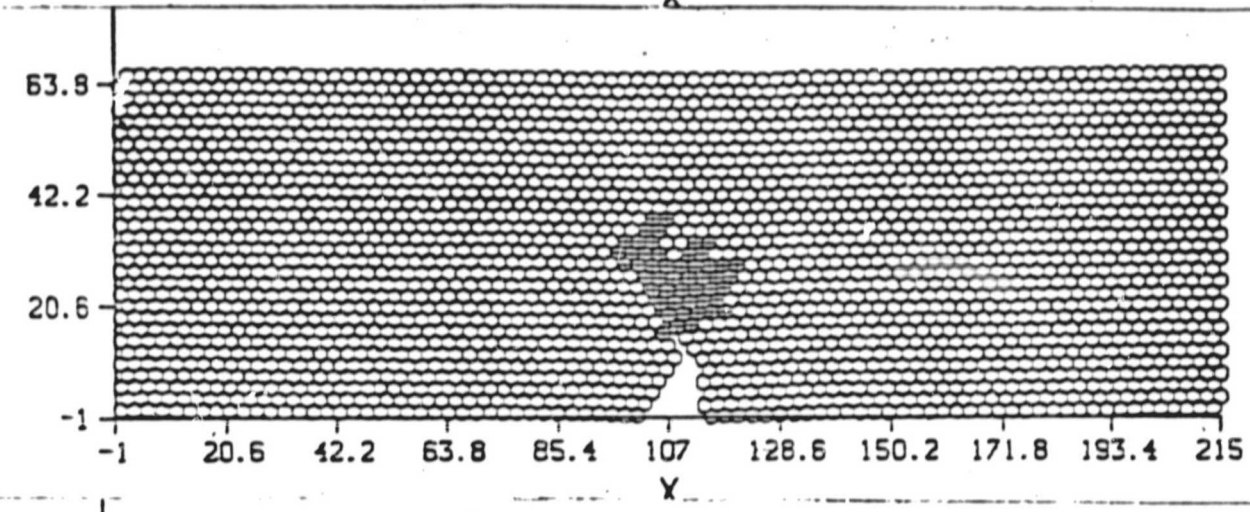

1400

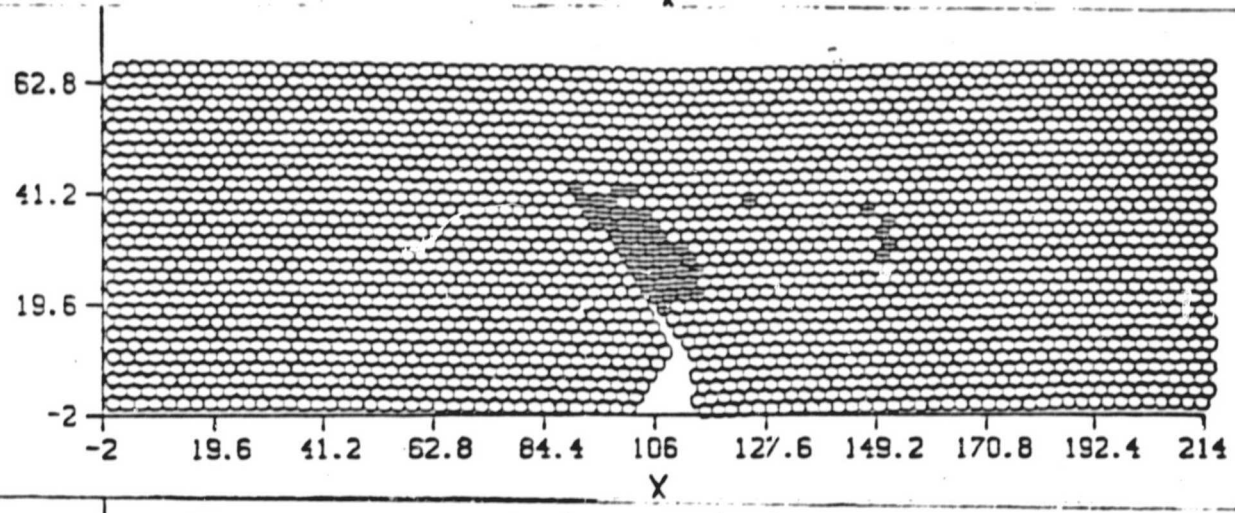

1600

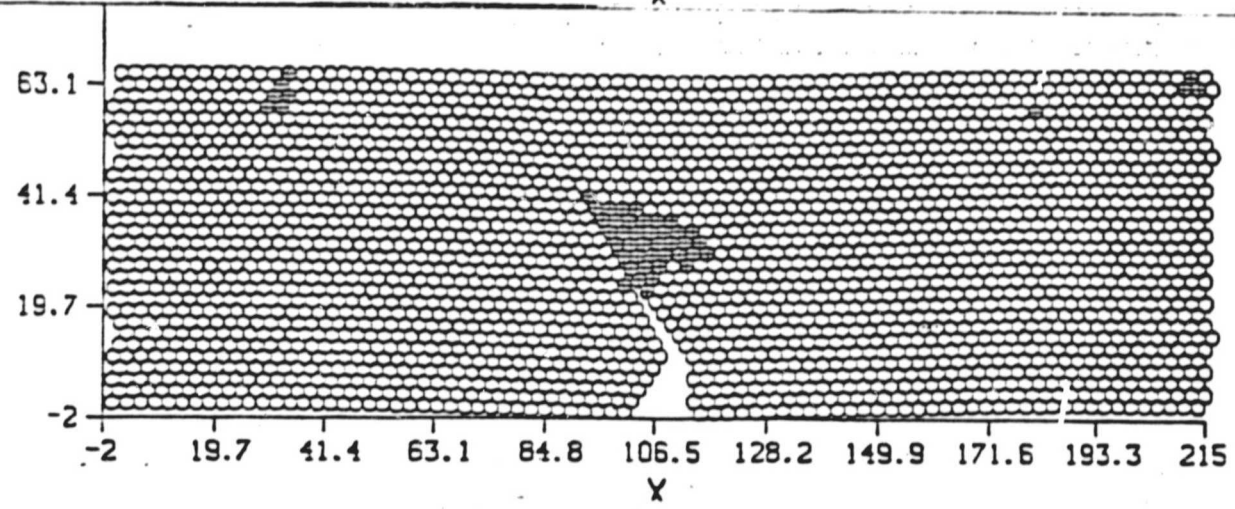

1800

Figure 4 (cont.)

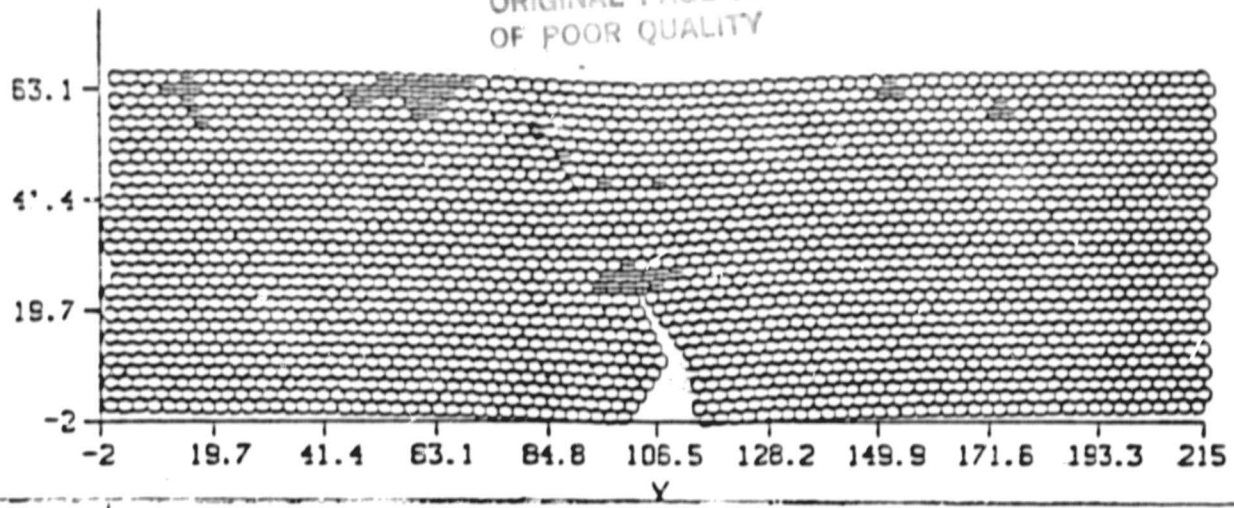

2000

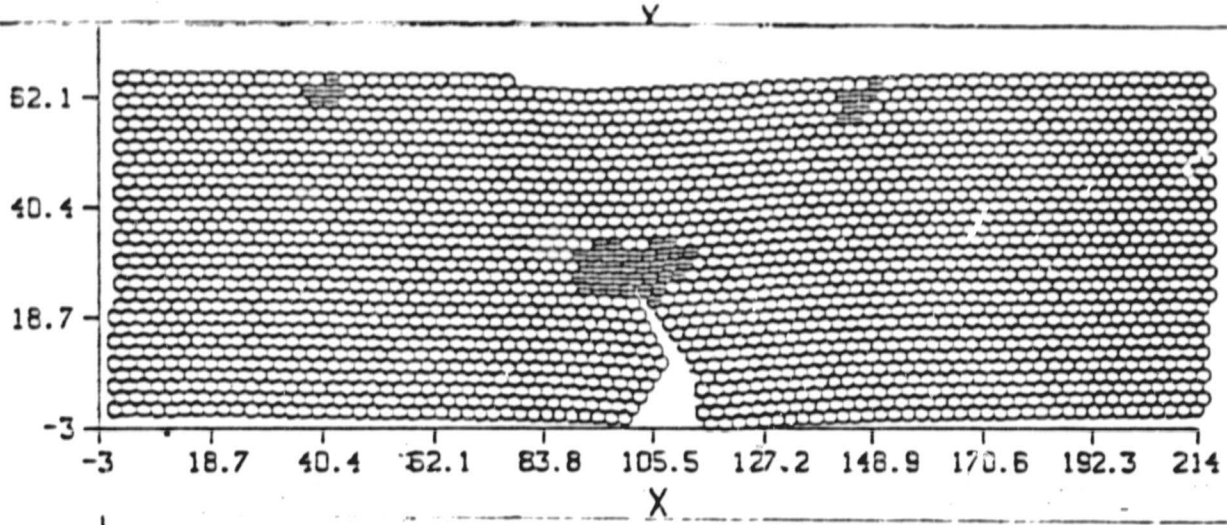

2200

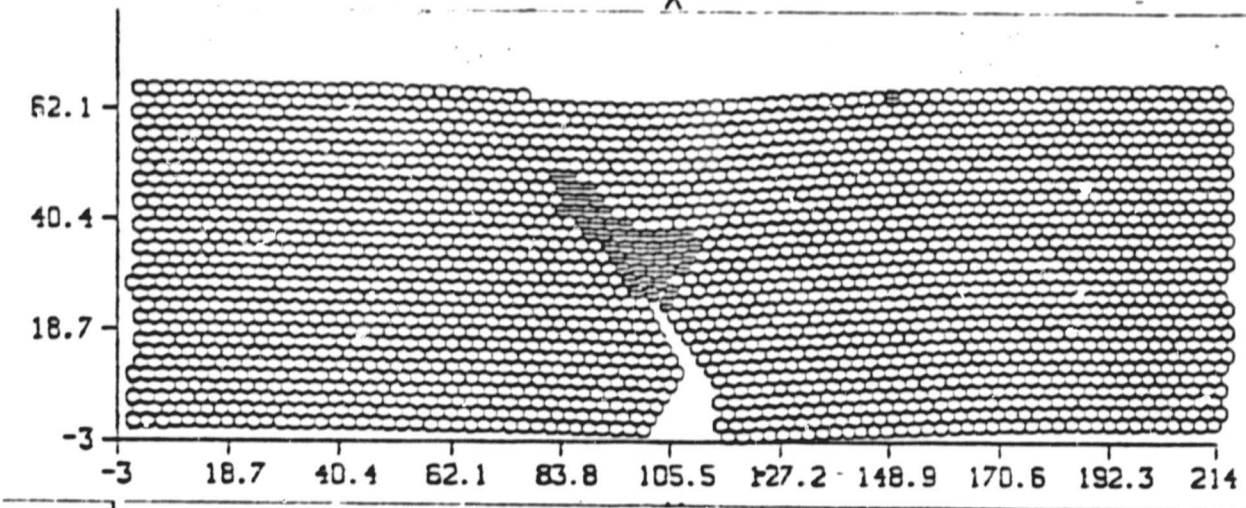

2400

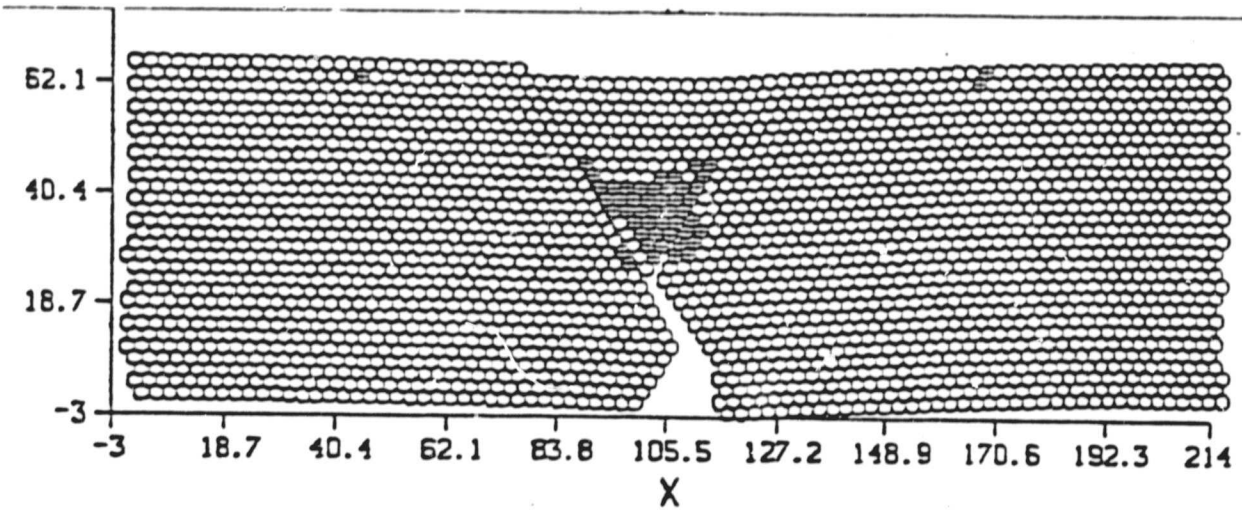

2600

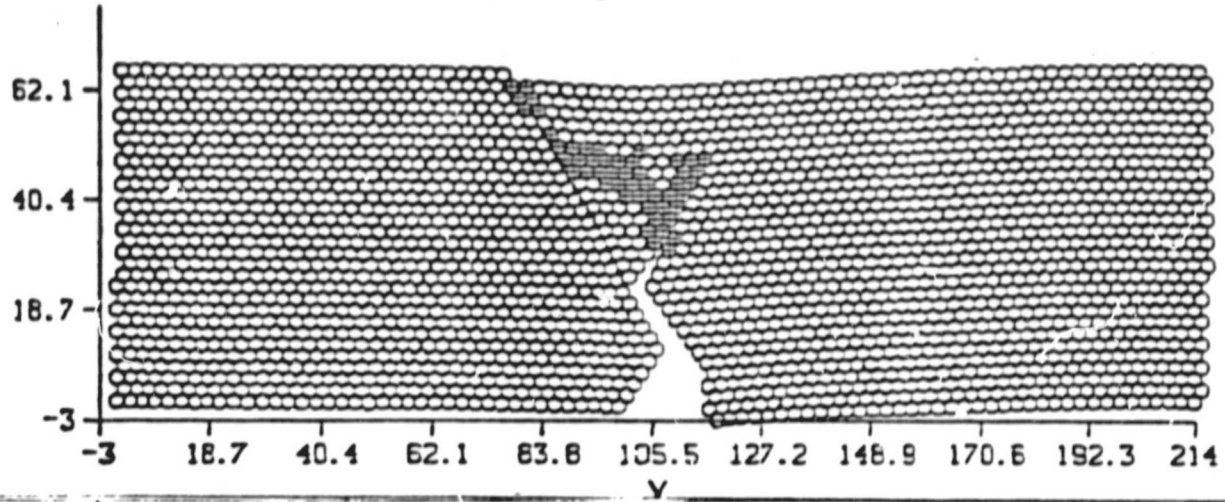

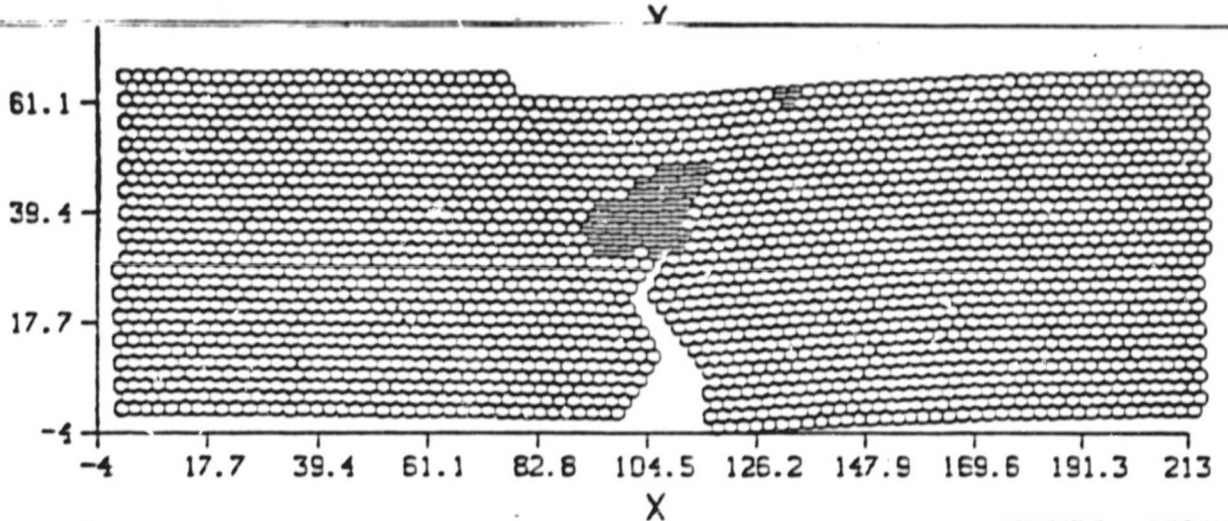

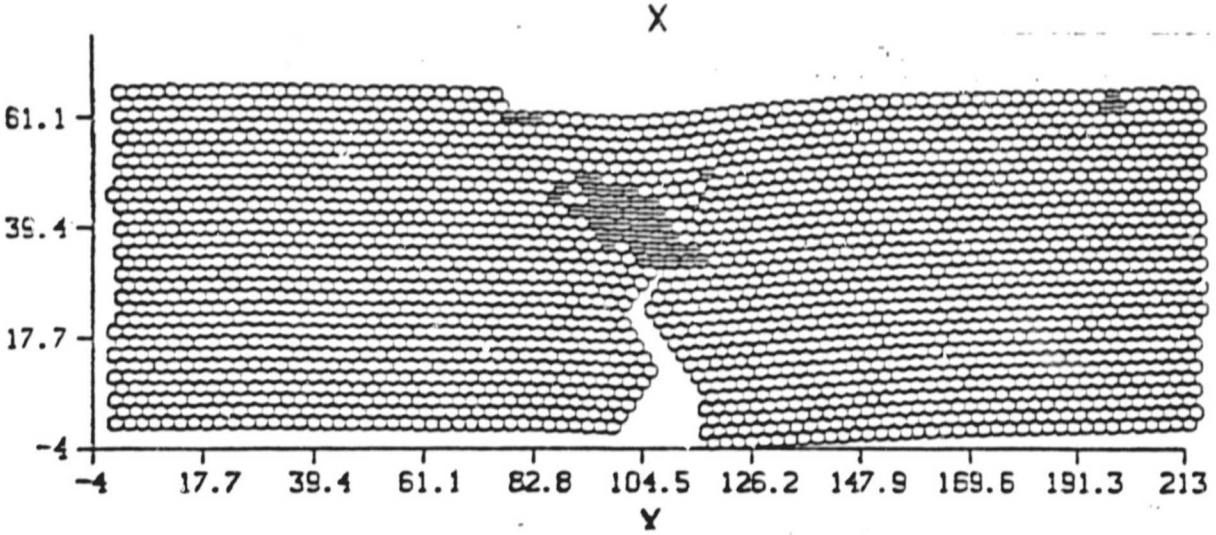

Figure 4 (

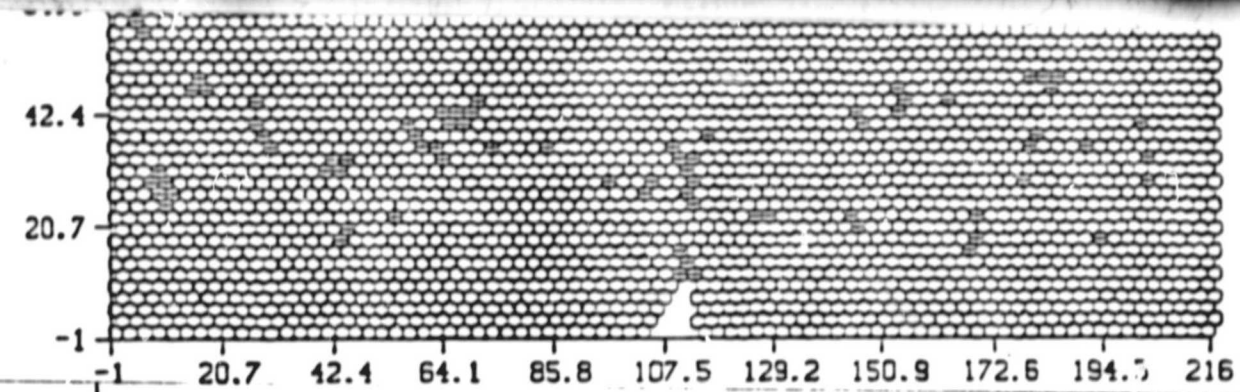

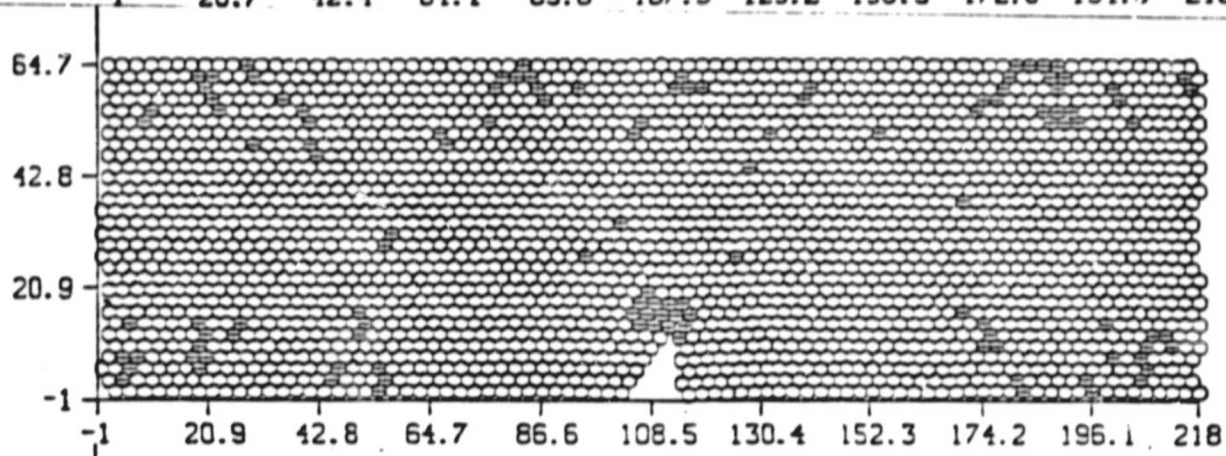

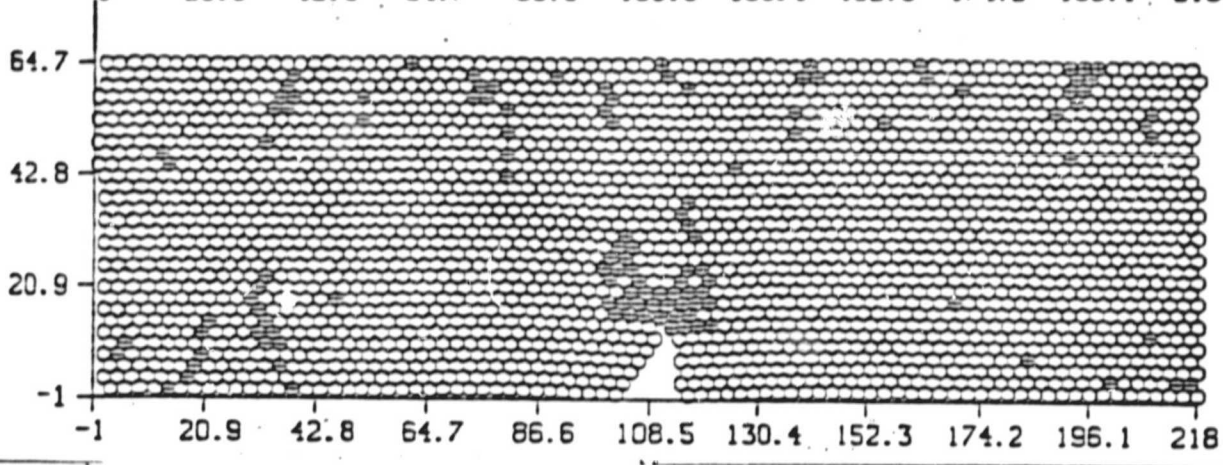

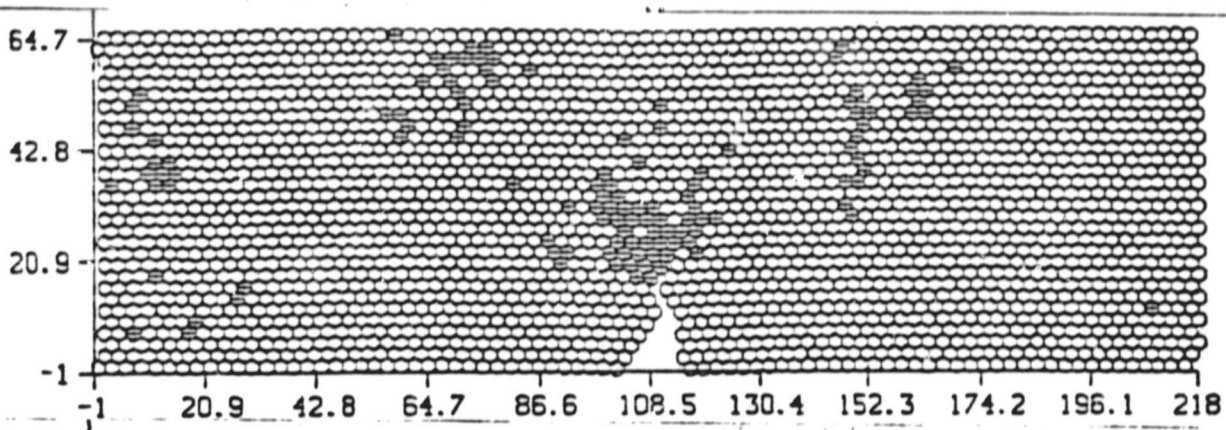

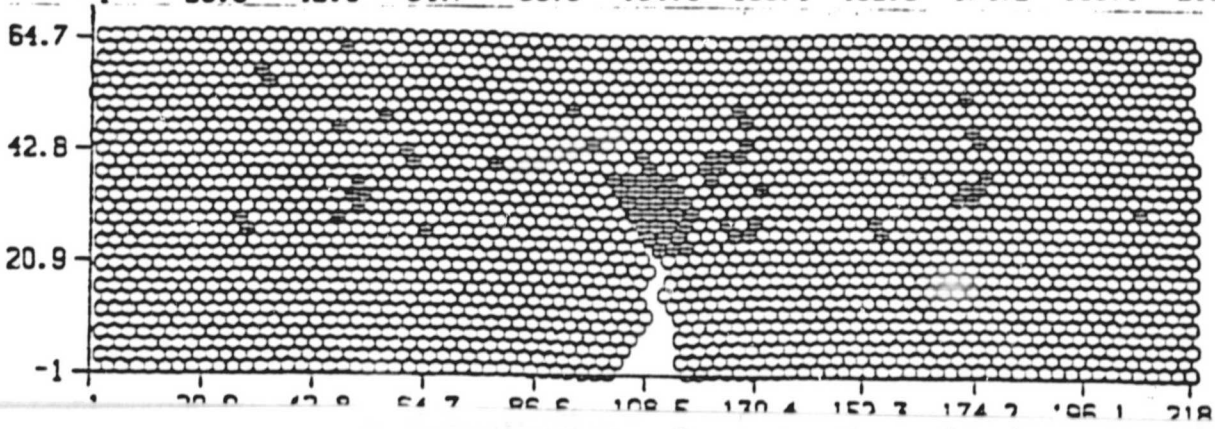

ORIGINAL PAGE IS
OF POOR QUALITY

Figure 5

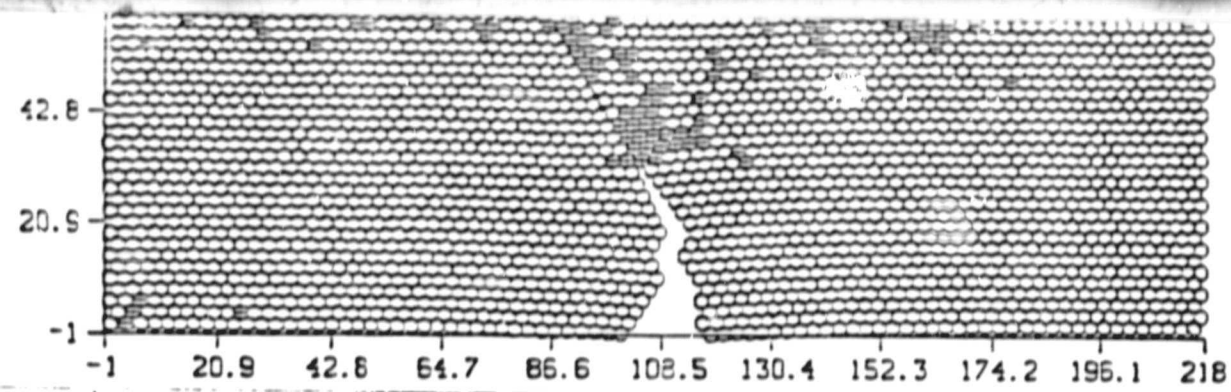

1200

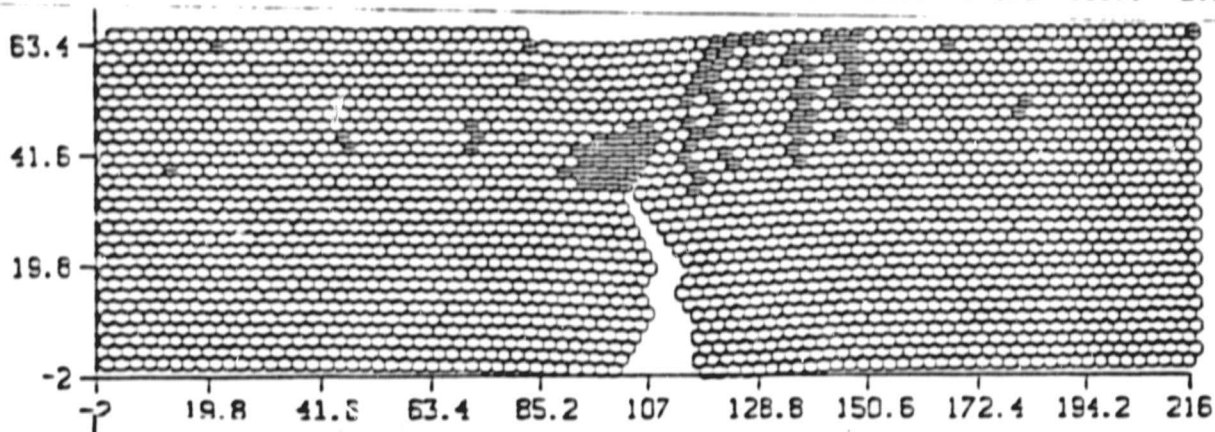

1400

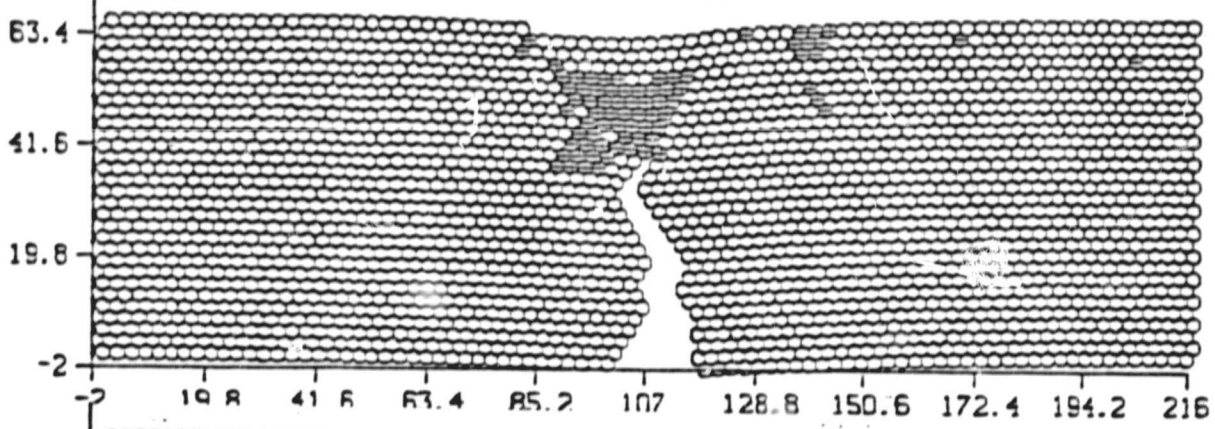

1600

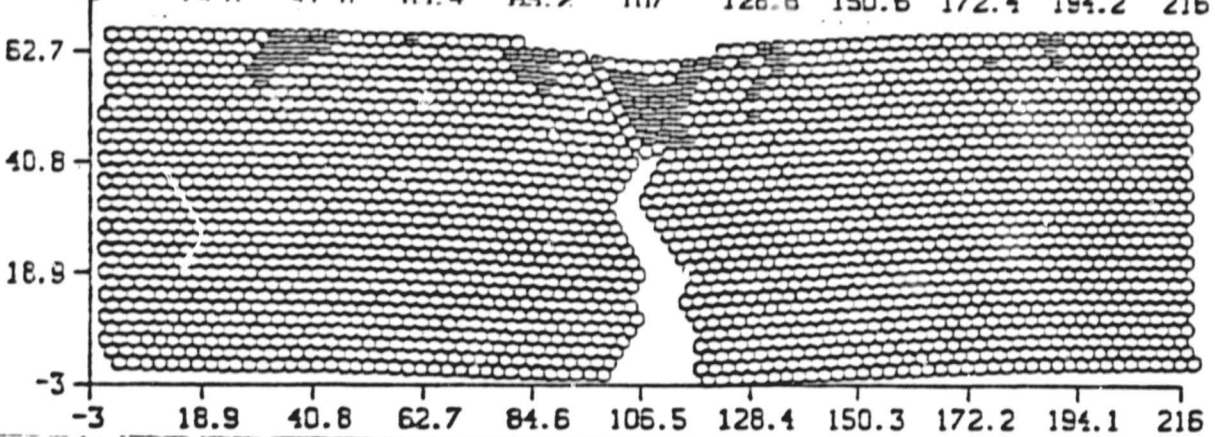

1900

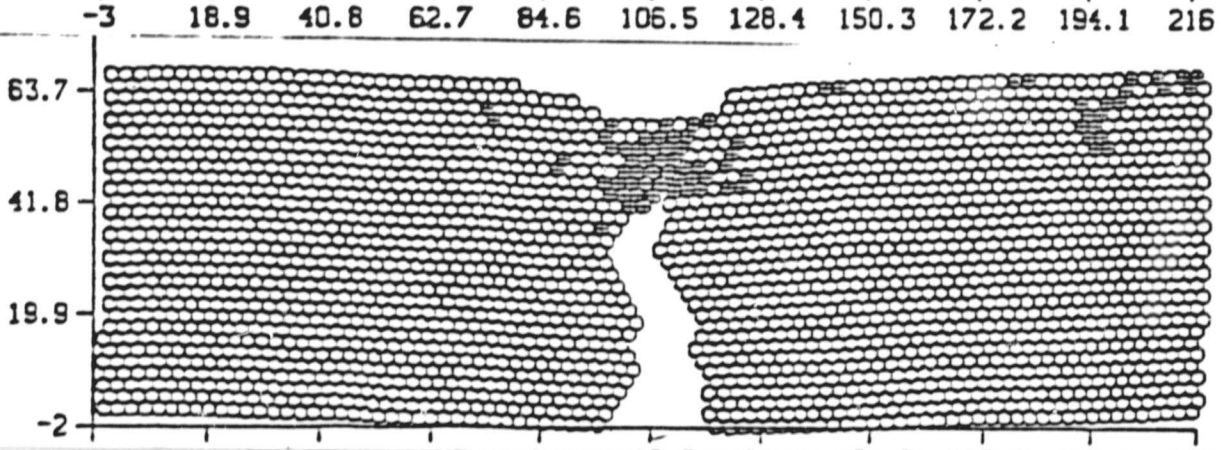

2400

Figure 5 (cont.)

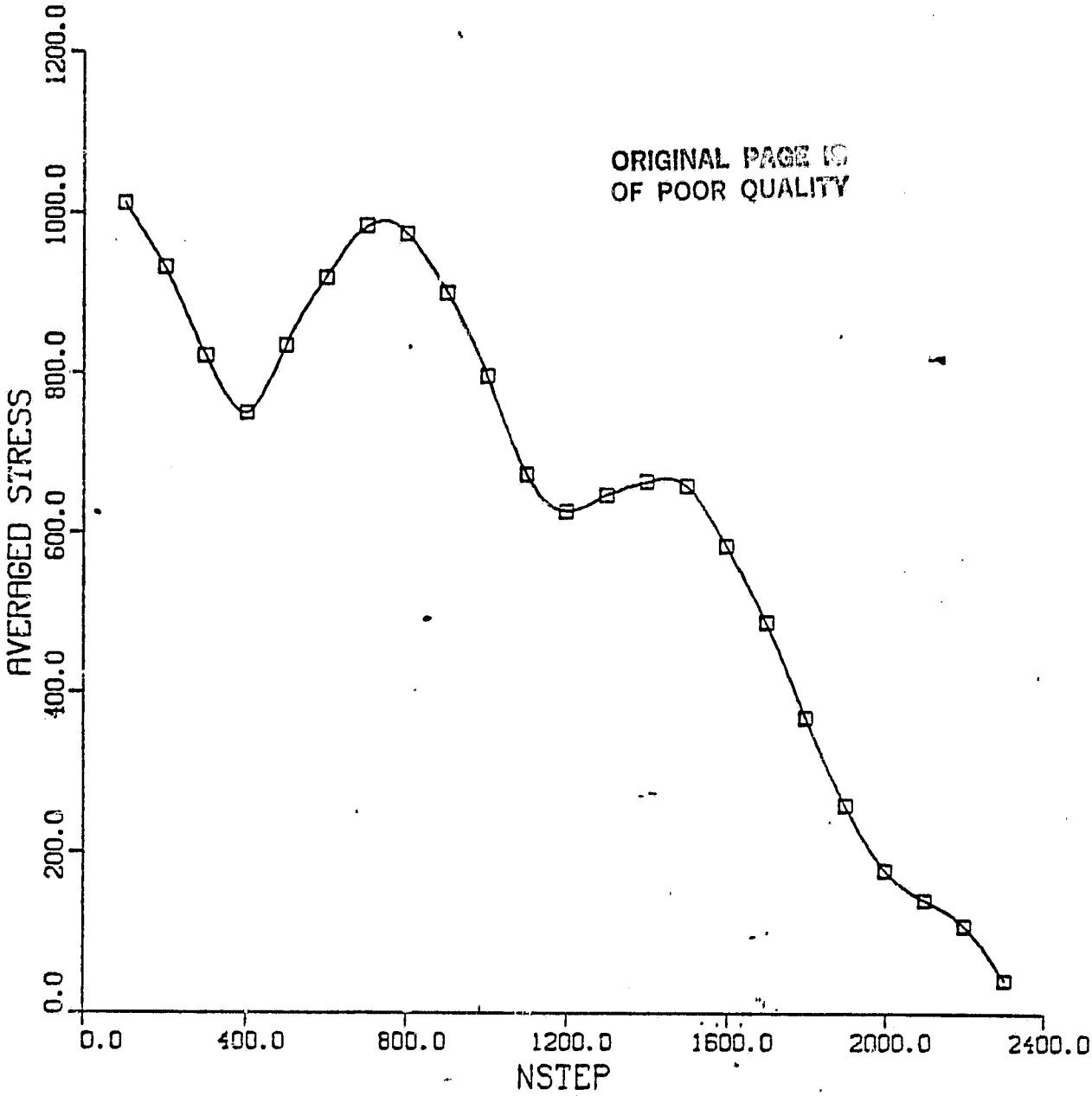
ORIGINAL PAGE IS
OF POOR QUALITY
AVERAGED STRESS
0.0
200.0
400.0
600.0
800.0
1000.0
1200.0
0.0
400.0
800.0
1200.0
1600.0
2000.0
2400.0
NSTEP

Figure 6.

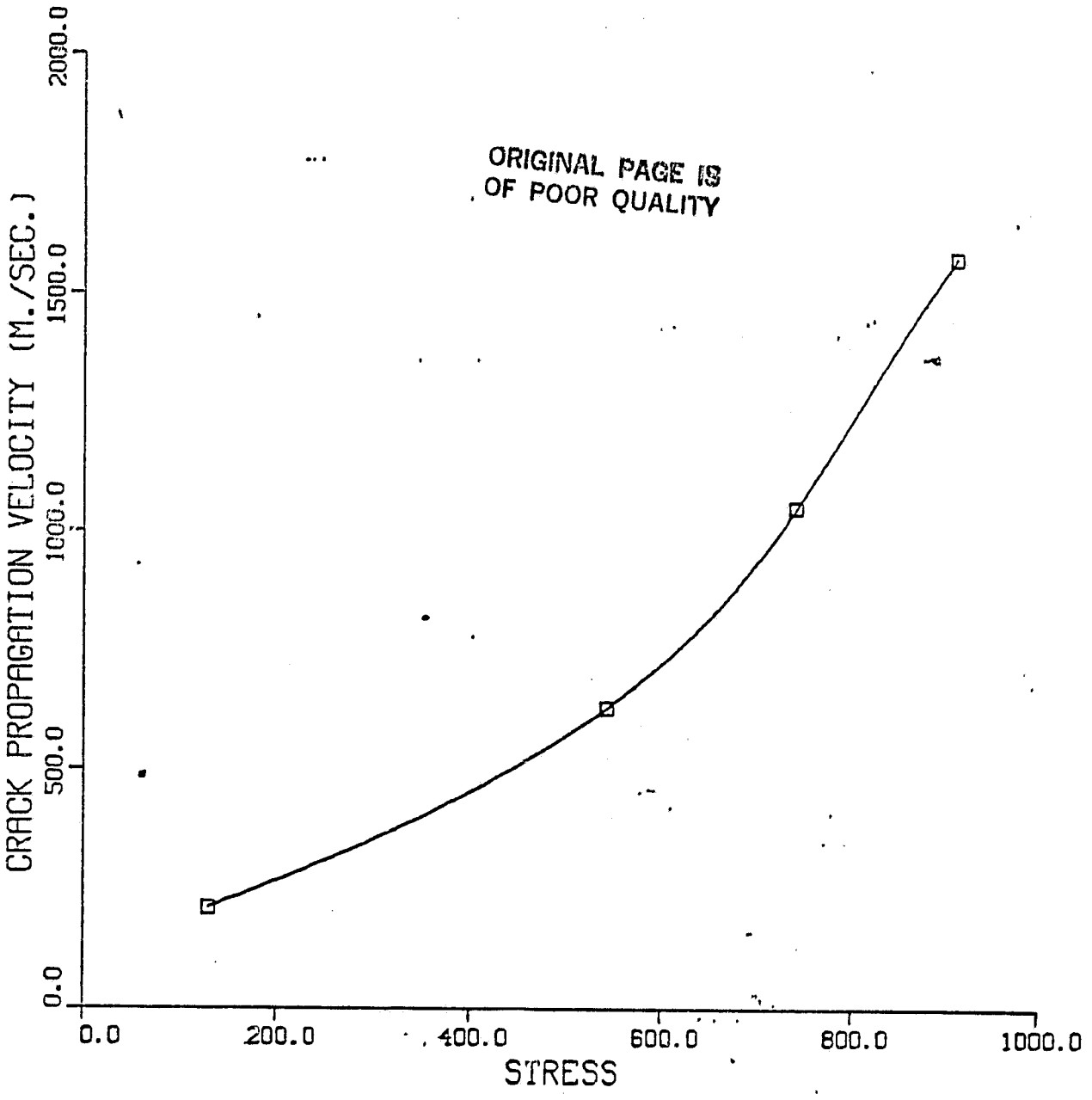

Figure 7.